

# Multi-level Second-order Few-shot Learning

Hongguang Zhang, Hongdong Li, and Piotr Koniusz

**Abstract**—We propose a Multi-level Second-order (MISo) few-shot learning network for supervised or unsupervised few-shot image classification and few-shot action recognition. We leverage so-called power-normalized second-order base learner streams combined with features that express multiple levels of visual abstraction, and we use self-supervised discriminating mechanisms. As Second-order Pooling (SoP) is popular in image recognition, we employ its basic element-wise variant in our pipeline. The goal of multi-level feature design is to extract feature representations at different layer-wise levels of CNN, realizing several levels of visual abstraction to achieve robust few-shot learning. As SoP can handle convolutional feature maps of varying spatial sizes, we also introduce image inputs at multiple spatial scales into MISo. To exploit the discriminative information from multi-level and multi-scale features, we develop a Feature Matching (FM) module that reweights their respective branches. We also introduce a self-supervised step, which is a discriminator of the spatial level and the scale of abstraction. Our pipeline is trained in an end-to-end manner. With a simple architecture, we demonstrate respectable results on standard datasets such as Omniglot, *mini*-ImageNet, *tiered*-ImageNet, Open MIC, fine-grained datasets such as CUB Birds, Stanford Dogs and Cars, and action recognition datasets such as HMDB51, UCF101, and *mini*-MIT.

**Index Terms**—Few-shot Learning, Second-order Statistics, Image Classification, Action Recognition

## I. INTRODUCTION

Convolutional Neural Networks (CNNs) have advanced a variety of models *e.g.*, object category recognition, scene classification and fine-grained image recognition. However, CNNs rely on large numbers of training labeled images and cannot be easily adapted to new tasks given very few samples. In contrast, the ability of humans to learn new visual concepts from very few examples highlights the superiority of biological vision. Thus, researchers study the so-called few-shot learning paradigm for which networks are trained or adapted to new concepts with few training samples. For example, recent few-shot learning approaches [84, 73, 78, 66] build on the notion of similarity learning [90, 33, 19]. In this paper, we study the one- and few-shot learning problems, and we focus on a simple design capturing robust statistics for the purpose of similarity learning.

In what follows, we employ second-order statistics of datapoints, which have advanced the performance of numerous methods, including object recognition, texture categorization, action representation, and tracking [83, 58, 87, 17, 7, 38]. For example, in the popular region covariance descriptors [83], a

covariance matrix computed over multimodal features from image regions is used as an object representation for recognition and tracking. Covariance descriptors have been extended to many other applications [83, 58, 87, 17] including end-to-end training of CNNs, leading to state-of-art results on action recognition, texture classification, scene and fine-grained recognition [34, 35, 42]. As second-order representations capture correlation patterns of features, they are a powerful tool used in several recognition pipelines [22, 68, 49, 39, 42, 48, 59, 41, 37, 101].

A typical few-shot learning network consists of a backbone that generates image features, and a base learner that learns to classify the so-called query images (*c.f.* class labels). In this paper, we use a multi-level network to obtain multiple levels of feature abstraction based on second-order features. We leverage intermediate outputs from the backbone, which helps the pipeline capture relations between the query and support images at multiple levels of abstraction. We note that a cascaded network was used before by GoogLeNet [79] with the goal of image classification rather than the similarity learning in the few-shot regime, which is a novel learning scenario not explored before.

By analyzing the class-wise activation maps, we ascertain that the features extracted from different levels of the backbone generally describe objects with respect to their different visual properties. Thus, such complementary to each other activation maps improve modeling of object relations across different levels of abstraction. To this end, we leverage second-order statistics formed from features of multi-level network streams. Firstly, we form and pass such second-order representations via the so-called Power Normalization (PN) to prevent the so-called burstiness effect [42], a statistical uncertainty of feature counts. As second-order pooling can effectively process feature maps of different spatial resolutions, we also employ inputs at multiple spatial scales to improve the quality of matching between objects at various scales. Secondly, we apply a so-called Feature Matching module which determines the importance of each level of abstraction and scale per query-support pair. Subsequently, we form relationship descriptors and pass them to a so-called base learner which learns the similarity by comparing relationship descriptors (representing query-support pairs) via the Mean Square Error (MSE) loss. Finally, we refine the multi-level second-order matrices, each corresponding to some level of abstraction in the multi-level network, by applying a self-supervised pretext task [14, 20, 9] with the level and scale indexes used as auxiliary labels. Such a self-supervised step helps the multi-level network learn more distinctive and complementary abstraction responses.

We apply our network to the few-shot image and action recognition tasks. In contrast to the large-scale object classification, few-shot learning requires an investigation into the ef-

H. Zhang\* is with Systems Engineering Institute, AMS. H. Li and P. Koniusz are with the College of Engineering and Computer Science, Australian National University. P. Koniusz is also with Data61/CSIRO. E-mail: [zhang.hongguang@outlook.com](mailto:zhang.hongguang@outlook.com), [hongdong.li@anu.edu.au](mailto:hongdong.li@anu.edu.au), [piotr.koniusz@data61.csiro.au](mailto:piotr.koniusz@data61.csiro.au). Code: <https://github.com/HongguangZhang/mlso-tmm-master>.

This work is supported by National Natural Science Foundation of China (Grant No. 62106282), and Equipment Development Research Fund (Grant No. ZX2020C2316).

Part of this work was done during H. Zhang's stay at the ANU. Manuscript received May 12, 2021, accepted Jan. 9, 2022. DOI: <https://doi.org/10.1109/TMM.2022.3142955>

fective use of multiple levels of feature abstraction, combined with second-order relationship descriptors, to determine the best performing architecture. As second-order statistics require appropriate pooling for such a new problem, we employ PN which is known to act as detector of visual features. PN discards the so-called nuisance variability (burstiness), the uncertainty of the frequency of specific visual features which vary unpredictably from image to image of the same class [42]. We speculate that, as we capture relationships between multiple images in a so-called episode, such a nuisance variability would be multiplicative w.r.t. the number of images per episode. PN limits such a harmful effect.

Our contributions are summarized below:

- i. We propose to generate scale-wise second-order representations at multiple levels of abstraction via a multi-level network, and we introduce the Feature Matching (FM) module to reweight the importance of each abstraction level and scale. FM selects the most discriminative pairs for relation learning. We show the importance of reweighting and matching across multiple spatial scales at multiple levels of feature abstraction.
- ii. We investigate how to build second-order relational descriptors from feature maps to capture the similarity between query-support pairs for few-shot learning.
- iii. We develop a self-supervised discriminator acting on scale-wise second-order representations of multiple levels of abstraction whose role is to predict the index of abstraction and scale, thus improving the complementarity and distinctiveness between different abstraction levels and scales.

To the best of our knowledge, we are the first to investigate multiple levels of feature abstraction, multiple input scales, and self-supervision for one- and few-shot learning. In this work, we build upon the SoSN model [97], the first few-shot learning model successfully leveraging second-order pooling.

## II. RELATED WORK

Below, we describe popular one- and few-shot learning models, and discuss other related topics.

### A. Learning From Few Samples

The ability of ‘*learning quickly from only a few examples is definitely the desired characteristic to emulate in any brain-like system*’ [60]. This desired principle poses a challenge to CNNs which typically leverage large-scale datasets [64]. Current trends in computer vision highlight the need for the ‘*ability of a system to recognize and apply knowledge and skills learned in previous tasks to novel tasks or new domains, which share some commonality*’. For one- and few-shot learning, a robust ‘*transfer of particle*’, introduced in 1901 by Woodworth [91], is also a desired mechanism because generalizing based on one or few datapoints to account for intra-class variability of thousands images is formidable.

**One- and Few-shot Learning (FSL)** have been studied in computer vision in both shallow [12, 2, 11, 45] and deep learning scenarios [32, 84, 73, 13, 78, 107, 24, 23, 57, 69,

80, 56, 25, 94]. For brevity, we review only the deep learning techniques. Siamese Network [32], a CNN based on two-streams, generates image descriptors and learns the similarity between them. Matching Network [84] introduces the concept of the support set, and the  $L$ -way  $Z$ -shot learning protocols. Matching Network captures the similarity between a query and several support images, and generalizes well to previously unseen test classes. Prototypical Networks [73] learn a model that computes distances between a datapoint and prototype representations of each class. Model-Agnostic Meta-Learning (MAML) [13] and Task-Agnostic Meta-Learning (TAML) perform a rapid adaptation to new tasks via meta-learning. Moreover, a large family of meta-learning approaches apply some form of the gradient correction *e.g.*, Meta-SGD [47], MAML++ [1], Reptile [53], CAVIA [108] LEO [65] and ModGrad [72] adapt the step-size of the gradient updates. Relation Net [78] learns the relationship between query and support images by leveraging a similarity learning network wired with the backbone. Note that relationship learning in few-shot learning is closely related to metric learning [90, 33] rather than relationship learning in graphs [82, 88]. SalNet [99] is an efficient saliency-guided end-to-end meta-hallucination approach. AFL [107] proposes a novel attribute-guided two-layer learning framework to improve the generalized performance of image representations. LRPABN [24] uses an effective low-rank pairwise bilinear pooling operation to capture the nuanced differences between images. FAML [57] proposes a novel GAN-based few-shot image generation approach, which is capable of generating new realistic images for unseen target classes in the low-sample regime. Zhu *et al.* [104] propose a novel global grouping metric to incorporate the global context, resulting in a per-channel modulation of local relation features. Moreover, a cross-modal retrieval can be performed by a modified meta-learning framework [74]. Finally, Graph Neural Networks (GNN) [30, 92, 31, 77, 103] have also been used in few-shot learning [67, 29, 16, 86], and achieved competitive results. Self-supervision has also been studied in few-shot learning [14, 76, 94, 98] where transformation-based auxiliary self-supervised classifiers are employed to improve the robustness of few-shot learning models. For instance, FLAT [94] uses a self-supervision strategy to pre-train the auto-encoder via the reconstruction of transformations applied to images, followed by training with the supervised loss.

Our pipeline is somewhat similar to Relation Net [78] and Prototypical Networks [73] in that we use the two basic building blocks underlying such approaches, that is, the feature encoder (or backbone) and the similarity learning network. However, Relation Net and Prototypical Net are first-order models which do not use multiple levels of feature abstraction. In contrast, we investigate second-order representations with PN to capture correlations of features. We also use multiple intermediate feature outputs to obtain different levels of feature abstraction. Our work builds on our SoSN model [97], which we extend in this work by adding multiple levels of feature abstraction, multi-scale inputs, a feature matching mechanism, and a self-supervision step. Finally, we also include an extension of our pipeline to the problem of few-shot action recognition.

**Few-shot Action Recognition (FSAR)** has been studied by the limited number of recent works [51, 18, 93, 105, 100, 86]. Though action recognition [70, 71, 81] has been studied for a long time, it remains a challenging problem under the few-shot setting. Mishra *et al.* [51] propose a generative framework for zero- and few-shot action recognition, by modeling each action class by a probability distribution. Guo *et al.* [18] leverage neural graph matching to learn to recognize previously unseen 3D action classes. Xu *et al.* [93] propose a dilated network to simultaneously capture local and long-term spatial temporal information. Zhu *et al.* [105] propose a novel compound memory network. Hu *et al.* [23] learn a dual-pooling GNN to improve the discriminative ability for selecting the representative video content and refine video relations. Finally, noteworthy are few-shot pipelines such as VideoPuzzle [8] which generates aesthetically enhanced long-shot videos from short video clips, and JEANIE [86] which performs FSAR on datasets of articulated human 3D body joints.

### B. Second-order Statistics/Power Normalization

Below we discuss several shallow and CNN-based methods which use second-order statistics. We conclude with details of so-called pooling and Power Normalization.

**Second-order statistics** have been used for texture recognition [83, 63] by so-called Region Covariance Descriptors (RCD) and further applied to tracking [58], semantic segmentation [7] and object category recognition [38, 39]. Co-occurrence patterns have also been used in the CNN setting. A recent approach [68] extracts feature vectors at two separate locations in feature maps to perform an outer product in a CNN co-occurrence layer. Higher-order statistics have also been used for action recognition from the body skeleton sequences [34, 37] and for domain adaptation [35]. In this work, we perform end-to-end training for one- and few-shot learning by the use of second-order relation descriptors (a novel proposition) that capture relations between the query and support images (or videos) before passing them to the similarity learning network. Second-order statistics have to deal with the so-called burstiness, ‘the property that a given visual element appears more times in an image than a statistically independent model would predict’ [26]. This is achieved by Power Normalization [40, 38] which is known to suppress this burstiness. PN has been extensively studied and evaluated in the context of Bag-of-Words [40, 38, 39] and category recognition with deep learning [42, 41].

A theoretical relation between Average and Max-pooling was studied in [5], which highlighted the underlying statistical reasons for the superior performance of max-pooling. A survey [40] showed that so-called MaxExp pooling in [4] acts as a detector of ‘at least one particular visual word being present in an image’, and thus it can be approximated with a simple  $\min_n(1, \eta \phi_{kn})$  for  $\eta > 0$ , whose variant we use in this paper.

## III. BACKGROUND

Below we detail our notations, and explain how to compute second-order statistics with PN.

**Notations.** Let  $\mathbf{x} \in \mathbb{R}^{d'}$  be a  $d'$ -dimensional feature vector.  $\mathcal{I}_N$  stands for the index set  $\{1, 2, \dots, N\}$ . We also define  $\mathbf{1} = [1, \dots, 1]^T$ . Operators  $\cdot_1, \cdot_2$  and  $\cdot_3$  denote concatenation of tensors along the first, second and third mode, respectively. Operator  $(\cdot)$  denotes vectorization of a matrix or tensor. Typically, capitalized bold symbols such as  $\Phi$  denote matrices, lowercase bold symbols such as  $\phi$  denote vectors, and regular symbols such as  $n$  or  $Z$  denote scalars. Also,  $\Phi_{ij}$  is the  $(i, j)$ -th coefficient of  $\Phi$ .

**Autocorrelation matrices.** The linearization of sum of Polynomial kernels results in two autocorrelation matrices.

**Proposition 1.** Let  $\Phi_A \equiv \{\phi_n\}_{n \in \mathcal{A}}$ ,  $\Phi_B \equiv \{\phi_n^*\}_{n \in \mathcal{B}}$  be datapoints from two images  $\Pi_A$  and  $\Pi_B$ , where  $N = |\mathcal{A}|$  and  $N^* = |\mathcal{B}|$  are the numbers of data vectors e.g., obtained from the last convolutional feature map of CNN for images  $\Pi_A$  and  $\Pi_B$ . Autocorrelation matrices emerge from the linearization of the sum of Polynomial kernels of degree 2:

$$K(\Phi_A, \Phi_B) = \langle \mathbf{F}(\Phi_A), \mathbf{F}(\Phi_B) \rangle = \frac{1}{NN^*} \sum_{n \in \mathcal{A}} \sum_{n' \in \mathcal{B}} \langle \phi_n, \phi_{n'}^* \rangle^2, \\ \text{where } \mathbf{F}(\Phi) = \frac{1}{N} \sum_{n \in \mathcal{A}} \phi_n \phi_n^T. \quad (1)$$

*Proof.* See [38, 39] for a derivation of this expansion.  $\square$

**Power Normalization.** In what follows, we use autocorrelation matrices with a pooling operator related to the following two propositions.

**Proposition 2.** Assume two event vectors  $\phi, \phi' \in \{0, 1\}^N$  which store the  $N$  trials each, performed according to the Bernoulli distribution under the i.i.d. assumption. Let  $p$  be the probability of an event ( $\phi_n \wedge \phi'_n = 1$ ) denoting a co-occurrence, and  $1-p$  of ( $\phi_n \wedge \phi'_n = 0$ ) denoting the lack of co-occurrence. Let  $p = \text{avg}_n \phi_n \phi'_n$  denote an expected value. Then the probability of at least one co-occurrence event ( $\phi_n \wedge \phi'_n = 1$ ) in  $\phi_n$  and  $\phi'_n$  simultaneously in  $N$  trials becomes  $\psi = 1 - (1-p)^\eta$  for  $\eta = N$ .

*Proof.* See [42] for a proof.  $\square$

**Proposition 3.** The first-order Taylor expansion of  $1 - (1-p)^\eta$  around  $p = 0$  and  $p = 1$  equals  $\eta p$  and  $1$ , respectively. Thus, we have  $1 - (1-p)^\eta \leq \min(\eta p, 1)$  on  $p \in [0; 1]$ . If we treat coefficients  $(i, j)$  of matrix  $\mathbf{M} = \Phi \Phi^T / \text{Tr}(\Phi \Phi^T)$  as approximately proportional to the co-occurrence probability of  $\phi_{in}$  and  $\phi_{jn}, \forall n \in \mathcal{S}_N$ , then for  $\Phi \geq 0$ , we obtain PN maps  $\Psi(\mathbf{M}; \eta) = \min(\eta \mathbf{M}, 1)$ , where  $\eta \approx N$  is an adjustable parameter accounting for the fact that we do not operate on the actual variable  $p$  drawn according to the Bernoulli distribution.

We adopt the above PN operator as it works well in practice according to survey [40]. Proposition 3 is a novel proposition.

## IV. PIPELINE

Below, we describe our network followed by our relationship descriptors whose role is to capture co-occurrences in the image and video representations. We also detail the Feature ENcoder (FEN) with multiple levels of abstraction outputs, the Feature Matching (FM) module and the self-supervised Visual Abstraction Level and Scale Discriminator.

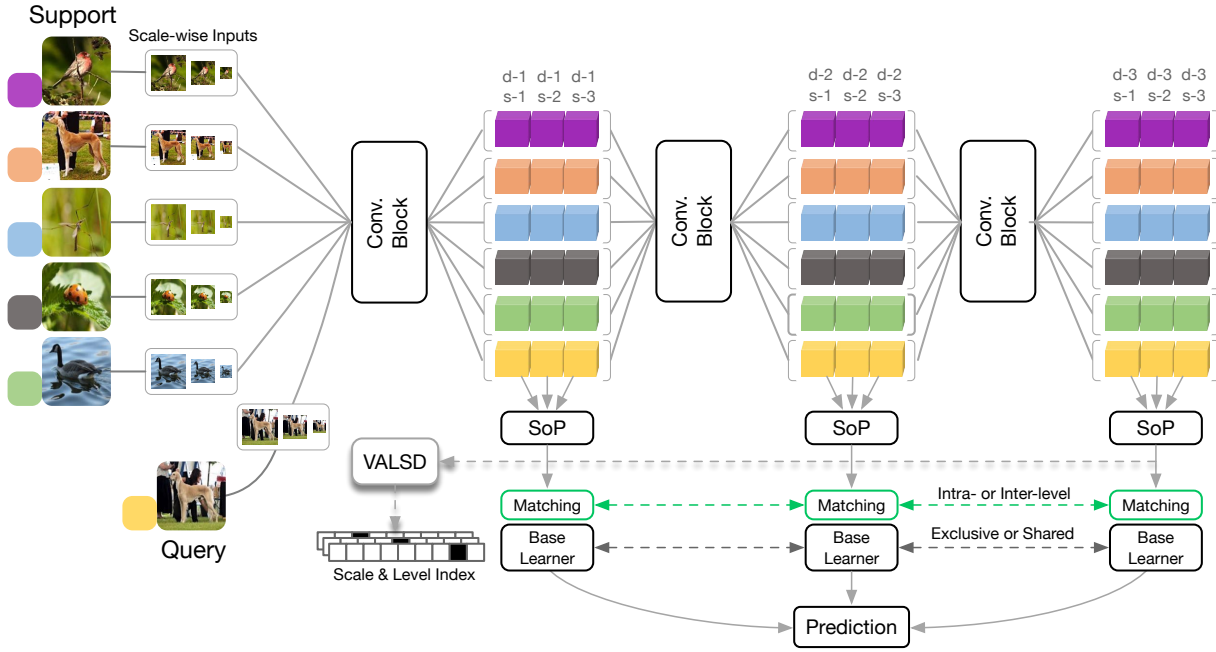


**Fig. 1:** The pipeline of our Multi-level Second-order (MISo) few-shot learning. Convolutional feature maps corresponding to inputs at multiple spatial scales are extracted at multiple levels of the CNN Feature Encoder to perform advanced matching. At each level, we apply second-order pooling with the Matching Module before passing these scale-wise representations to the base learner, with the MSE loss per level of visual abstraction applied, and the Visual Abstraction Level and Scale Discriminator.

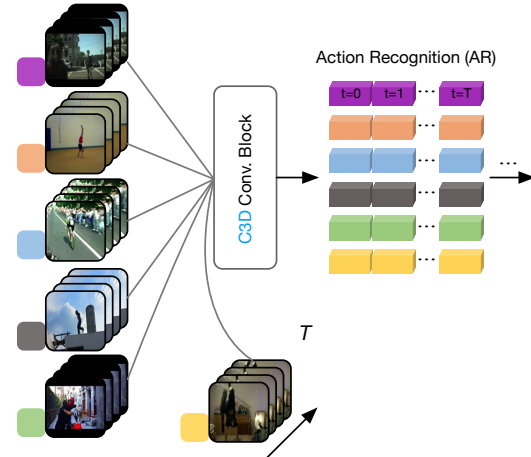


**Fig. 2:** For Few-shot Action Recognition, we use the C3D convolutional blocks and the second-order pooling which aggregates over the temporal mode (in addition to spatial locations of feature maps).

### A. Multi-level Second-order Few-shot Learning

Our Multi-level Second-order (MISo) few-shot learning pipeline, shown in Figure 1, consists of two major parts which are (i) the backbone (feature encoder, FEN) with multiple branches of features and (ii) the base learner *i.e.*, Similarity Network (SN), Logistic Regression (LR) or Nearest Neighbor (NN) classifier. The role of the backbone is to generate convolutional feature vectors which are then used as image descriptors. The base learner infers relations between query-support pairs. Our work differs from the Relation Net [78] in that we use multiple (*i.e.*, three) levels of feature abstraction

passed to second-order representations with PN, which form query-support relation descriptors. We feed such descriptors into SN for comparison of second- rather than the first-order statistics. For clarity, we first describe the Second-order Similarity Network which uses a single FEN output from the last layer. Subsequently, we explain the details of MISo.

**SoSN.** Let FEN be defined as an operator  $f: \mathbb{R}^{W \times H} \times \mathbb{R}^{|\mathcal{F}|} \rightarrow \mathbb{R}^{K \times N}$ , where  $W$  and  $H$  denote the width and height of an input image,  $K$  is the length of feature vectors (number of filters),  $N = N_W \cdot N_H$  is the total number of spatial locations in the last convolutional feature map. For simplicity, we denote an image descriptor by  $\Phi \in \mathbb{R}^{K \times N}$ , where  $\Phi = f(\mathbf{X}; \mathcal{F})$  for an image  $\mathbf{X} \in \mathbb{R}^{W \times H}$ , and  $\mathcal{F}$  are learnable parameters of the encoding network. The role of SN, denoted by  $r: \mathbb{R}^{K'} \times \mathbb{R}^{|\mathcal{R}|} \rightarrow \mathbb{R}$ , is to compare two datapoints encoded as some  $K'$  dimensional vectorized second-order representations. Typically, we write  $s(\psi; \mathcal{R})$ , where  $\psi \in \mathbb{R}^{K'}$ , whereas  $\mathcal{R}$  are learnable parameters of the similarity network. We define a relationship descriptor  $\vartheta: \mathbb{R}^{K \times N \times Z} \times \mathbb{R}^{K \times N} \rightarrow K'$  which captures some relationship between descriptors built from the  $Z$ -shot support images and a query image. This relationship is encoded via computing second-order autocorrelation matrices with PN for query and support embeddings, and forming some relation between query-support features *e.g.*, by concatenation, inner-product, subtraction, *etc.*, as explained later.

For the  $L$ -way  $Z$ -shot problem, assume that we have some support images  $\{\mathbf{X}_n\}_{n \in \mathcal{W}_1}$  from some set  $\mathcal{W}_1$  and their corresponding image descriptors  $\{\Phi_n\}_{n \in \mathcal{W}_1}$  form  $Z$ -shot relation descriptors. Moreover, assume that we have one query image  $\mathbf{X}^*$  with its image descriptor  $\Phi^*$  (the asterisk usually denotes query-related variables). Both the  $Z$ -shot and the

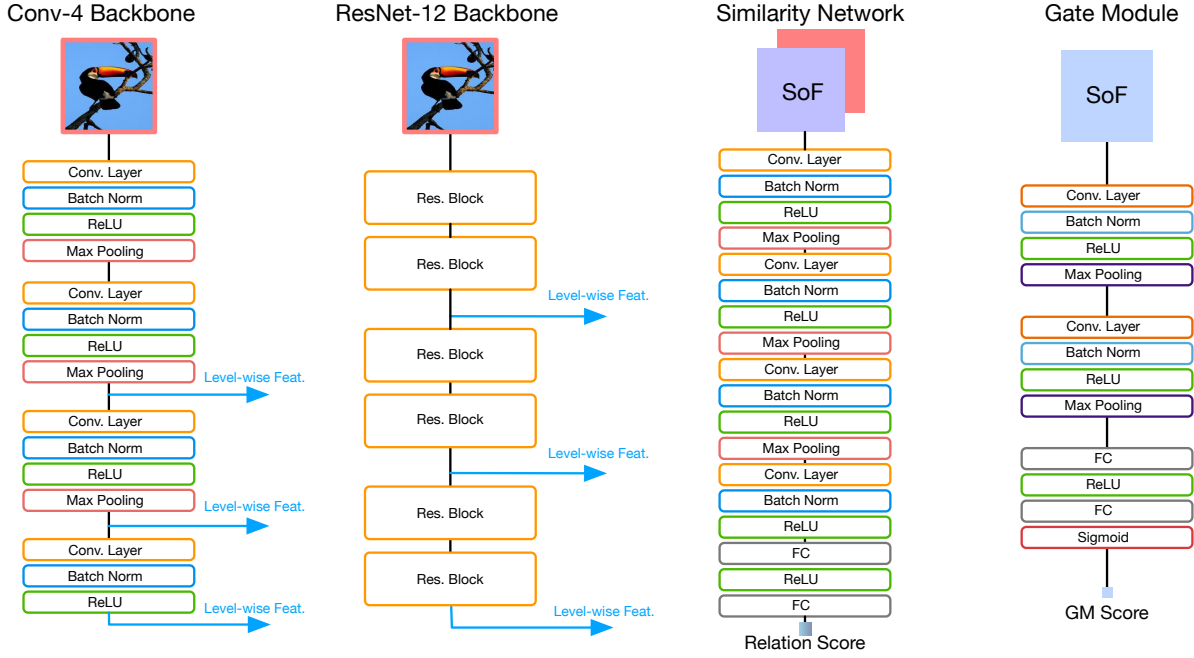


**Fig. 3:** The architecture of FEN (Conv-4 and ResNet-12 backbones), SN base learner, Gate Module employed in our approach.

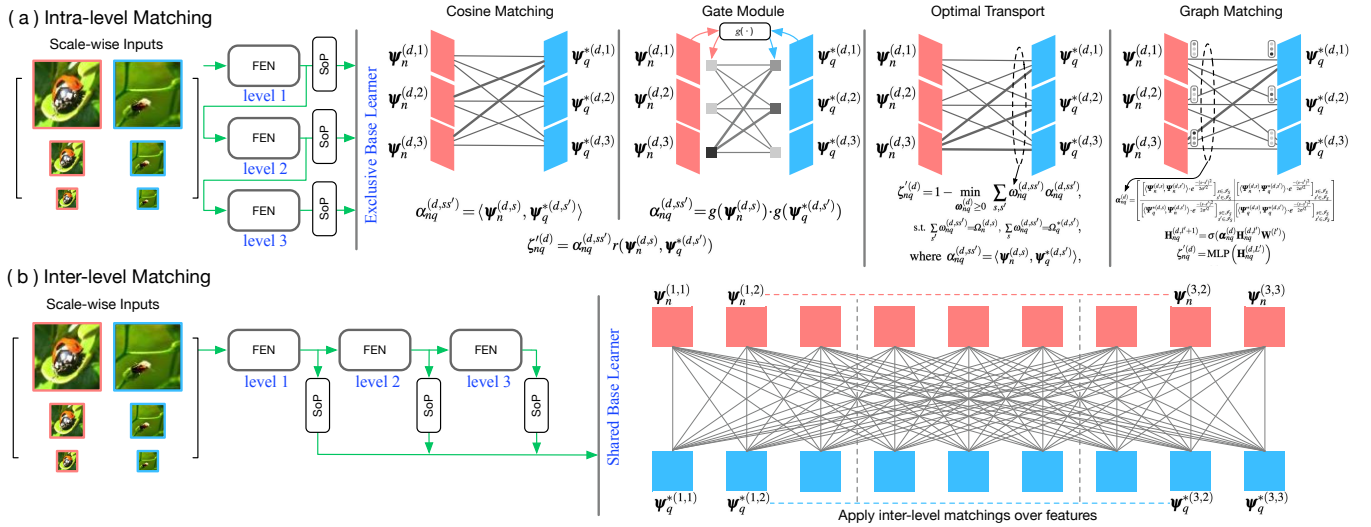


**Fig. 4:** Our matching strategies for multiple spatial scales and multiple levels of feature abstraction. Firstly, we downsample the original support and query images (or videos) to 1/2 or 1/4 of the original resolution. Subsequently, we feed them into the Feature Encoder and construct scale-wise support-query pairs for relation learning. Cosine Matching, Gate Module, Optimal Transport and Graph Matching strategies are detailed in Section IV-C.

query embeddings belong to one of  $L$  classes in the subset  $\mathcal{C}^\ddagger \equiv \{c_1, \dots, c_L\} \subset \mathcal{I}_C \equiv \mathcal{C}$ . Specifically, for an  $L$ -way problem, one obtains  $L$  relation descriptors, where one of  $L$  descriptors contains query-support pair of the same class, whereas the remaining  $L-1$  relation descriptors contain non-matching query-support classes. The  $L$ -way  $Z$ -shot learning step can be defined as learning the similarity w.r.t. relation descriptors:

$$\zeta_{lq} = r(\vartheta([\Phi_n]_{n \in \mathcal{W}_l}, \Phi_q^*), \mathcal{R}), \quad (2)$$

where  $\Phi_n = f(\mathbf{X}_n; \mathcal{F})$  and  $\Phi_q^* = f(\mathbf{X}_q^*; \mathcal{F})$ ,

where operator  $[\cdot]$  stacks matrices along the third mode,

support subsets and query are  $(\mathcal{W}_1, \dots, \mathcal{W}_L, q) \in \mathcal{E}$ , where  $\mathcal{E}$  is a set of episodes. Each  $\mathcal{W}_1$  shares the label with  $q$ , whereas  $\mathcal{W}_2, \dots, \mathcal{W}_L$  do not share the label with  $q$ . We use the Mean Square Error (MSE) for the objective of our end-to-end SoSN:

$$\arg \min_{\mathcal{F}, \mathcal{R}} \mathbb{E}_{(\mathcal{W}_1, \dots, \mathcal{W}_L, q) \sim \mathcal{E}} \sum_{1 \in \mathcal{I}_L} (\zeta_{lq} - \delta(c_l - c_q^*))^2, \quad (3)$$

where  $c_l$  are labels of support subsets and the query label  $c_q^*$  is always set as  $c_1$  (so that the query image has the same label as the first support subset),  $\delta(c_l - c_q^*)$  equals 1 if  $c_l = c_q^*$ , 0 otherwise.

For FSAR, we propose a C3D Second-order Similarity Network (C3D SoSN) that is equipped with FEN with C3D

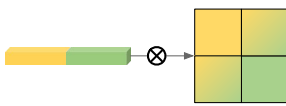
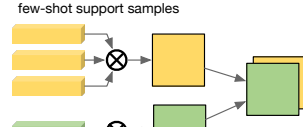
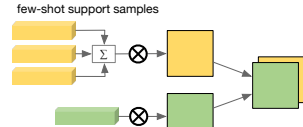
Operator	( $\otimes$ +F) Full single auto-correlation per support-query concatenated feature vectors.	( $\otimes$ +R) Rank differing auto-correlations, one per support, one per query, followed by the concatenation.	( $\otimes$ ) Auto-correlations, one per support, averaged over shots $\Phi$ , one per query, followed by the concatenation.
$\vartheta(\cdot) =$	 $\Psi\left(\frac{\bar{\Phi}\bar{\Phi}^T}{\text{Tr}(\bar{\Phi}\bar{\Phi}^T)}\right)_{(c)}$ <p>where <math>\bar{\Phi} = [\Phi_{n:1} \ \Phi^*]_{n \in \mathcal{W}_l}</math> (10)</p>	 $\left[ \begin{array}{c} \Psi\left(\frac{\bar{\Phi}\bar{\Phi}^T}{\text{Tr}(\bar{\Phi}\bar{\Phi}^T)}\right)_{:3} \\ \Psi\left(\frac{\Phi^*\Phi^{*T}}{\text{Tr}(\Phi^*\Phi^{*T})}\right)_{(c)} \end{array} \right]$ <p>where <math>\bar{\Phi} = [\Phi_n]_{n \in \mathcal{W}_l}</math> (11)</p>	 $\left[ \begin{array}{c} \Psi\left(\frac{\Phi\Phi^T}{\text{Tr}(\Phi\Phi^T)}\right)_{:3} \\ \Psi\left(\frac{\Phi^*\Phi^{*T}}{\text{Tr}(\Phi^*\Phi^{*T})}\right)_{(c)} \end{array} \right]$ <p>where <math>\bar{\Phi} = \sum_{n \in \mathcal{W}_l} \Phi_n</math> (12)</p>

TABLE I: Proposed relationship descriptors  $\vartheta$  used in relation learning. Note differences between equations (10), (11) and (12).

convolutional blocks, as in Figure 2. Firstly, we obtain C3D-based FEN embeddings over a video and then we compute the autocorrelation matrix with PN to obtain relation descriptors for query-support video pairs. We consider C3D SoSN as a baseline FSAR model. Thus, we do not investigate here any elaborate aggregation strategies, and we do not use the optical flow. However, we believe that further improvements over the C3D SoSN baseline can be easily achieved.

### B. Relationship Descriptor $\vartheta$

Table I offers some choices for the operator  $\vartheta$  whose role is to capture and summarize the information stored in query-support embeddings of image or video pairs. Such a summary is then passed to SN for learning to compare query-support pairs. Operator ( $\otimes$ +F) concatenates the support and query feature vectors prior to the outer-product step. Operator ( $\otimes$ +R) performs the outer-product on the support and query feature vectors separately prior to concatenation step along the third mode. Operator ( $\otimes$ ) averages over embeddings of  $Z$  support images from a given  $\mathcal{W}_l$ , followed by the outer-product step on the mean support and query vectors, and the concatenation step along the third mode.

### C. Multi-level Relation Learning

It is generally known that different layers of CNN are able to capture different kinds of visual abstraction *e.g.*, early layers may respond to edges, blobs and texture patterns, whereas deeper layers may respond to parts of objects under some small deformations. Therefore, we propose the Multi-level Second-order Similarity Network whose goal is to learn the similarity between query-support image or video pairs. To this end, we leverage the multiple levels of visual abstraction to learn object relations based on fine-to-coarse embeddings of images (or videos).

The architecture of MISo is shown in Figure 1. In contrast to SoSN which uses the final output of FEN as embeddings, MISo extracts feature vectors across fine-to-coarse levels that correspond to consecutive convolutional blocks, and forms autocorrelation matrices with PN and GM to produce the corresponding feature representations at multiple levels. Subsequently, an autocorrelation matrix per level is passed to SN with the goal of computing the relation scores which are fused to make the final prediction. Figure 5 visualizes

class activation maps at three different levels of FEN (ResNet-12 backbone) to demonstrate the complementary nature of activated regions. The figure shows that each level of visual abstraction in MISo responds differently to the same visual stimulus.

Subsequently, we employ SN learners with parameters  $\mathcal{R}_d, d \in \mathcal{S}_D$ , to learn the relations between query-support pairs for each level of abstraction. The  $L$ -way  $Z$ -shot learning step over  $D$  levels of feature abstraction can be redefined as learning the similarity w.r.t. relation descriptors:

$$\zeta_{lq}^{(d)} = r\left(\vartheta\left([\Phi_n^{(d)}]_{n \in \mathcal{W}_l}, \Phi_q^{*(d)}\right), \mathcal{R}_d\right), \quad (4)$$

where  $\Phi_n^{(d)} = f^{(d)}(\mathbf{X}_n; \mathcal{F})$  and  $\Phi_q^{*(d)} = f^{(d)}(\mathbf{X}_q^*; \mathcal{F})$ ,

with the following MSE loss:

$$\arg \min_{\mathcal{F}, \mathcal{R}_1, \dots, \mathcal{R}_D} L_R, \quad (5)$$

where  $L_R = \mathbb{E}_{(\mathcal{W}_1, \dots, \mathcal{W}_L, q) \sim \mathcal{E}} \sum_{l \in \mathcal{S}_L} \sum_{d \in \mathcal{S}_D} \left(\zeta_{lq}^{(d)} - \delta(c_l - c_q^*)\right)^2$ ,

and the label-related symbols are defined as for Eq. (3). During the inference step, we average the individual classifier votes obtained from multiple levels of feature abstraction. We determine the final class  $c_q^*$  for a given testing episode  $(\mathcal{W}_1, \dots, \mathcal{W}_L, q) \sim \mathcal{E}_{test}$  as follows:

$$c_q^* = c_{l'} \quad \text{where } l' = \arg \min_{l \in \mathcal{S}_L} \sum_{d \in \mathcal{S}_D} \left(S_{lq}^{(d)} - 1\right)^2. \quad (6)$$

**Scale-wise Boosting (SB).** Below we demonstrate how the inputs at multiple spatial scales are utilized by our multi-level network. The use of scale-wise inputs is shown in Figure 1. Given a pair of support and query images,  $\mathbf{X}_n$  and  $\mathbf{X}_q^*$ , we first downsample them to obtain the multi-scale inputs,  $\mathbf{X}_n^{(s)}$  and  $\mathbf{X}_q^{*(s')}$ . Then we feed them into the feature encoder to generate the convolutional features  $\Phi^{(s)}$  and  $\Phi^{*(s')}$ , where  $s$  and  $s'$  are scale-wise indexes. Subsequently, we form the support-query relation descriptors at spatial scales  $(s, s')$ , pass them via function  $r$ , and obtain the scale-wise relation similarity scores  $\zeta_{lq}^{(ss')}$ :

$$\zeta_{lq}^{(ss')} = r(\vartheta(\Phi_n^s, \Phi_q^{*s'}), \mathcal{R}), \quad (7)$$

where  $s, s' \in \mathcal{S}_S$  are the scale indexes ranging from 1 to 3, referring to inputs at 1, 1/2 and 1/4 of the original resolution. The number of scales we use is  $S=3$ .

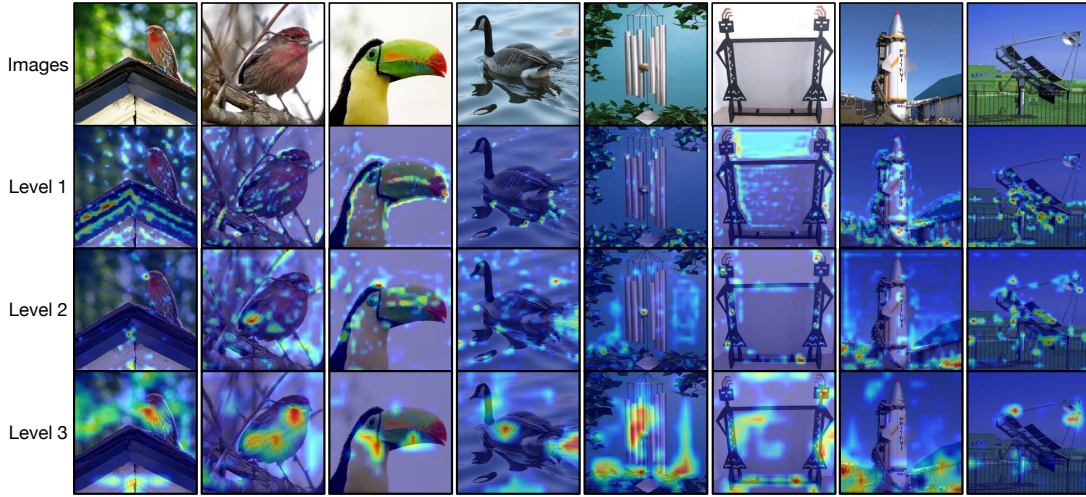


**Fig. 5:** Visualization of features at several levels of abstraction. We indicate the Gate Module scores (GM) in the right bottom corner per image. We use ResNet-12 FEN of MISo to obtain features with the CAM [102] visualization model on images of *mini-ImageNet*. The class-wise activation maps vary at different levels of abstraction. Given animals in rows 1–4, shallower features are localized at boundaries between the object and background. More abstract features appear on salient fine-grained parts of animals. For images of aerospace airplanes and radars, shallower features come from objects, whereas more abstract features capture salient parts of objects or the context around them. Therefore, multiple levels of abstraction provide complementary descriptions of various visual concepts.

As  $\zeta_{lq}^{(ss')}$  is the similarity between  $\mathbf{X}_n$  and  $\mathbf{X}_q^*$  at scales  $s$  and  $s'$ , the remaining part of the pipeline may deal with the scale-wise matching of objects in various ways. Note that the scale-wise matching deals with the scale variations of objects, whereas the feature abstraction relates to the level of semantic composition. Thus, both strategies may be combined to improve the few-shot learning step.

Below is a simple extension of our pipeline to a variant with multiple levels of abstraction and multiple spatial scales:

$$\zeta_{lq}^{(d,ss')} = r\left(\mathcal{D}\left([\Phi_n^{(d,s)}]_{n \in \mathcal{W}_l}, \Phi_q^{*(d,s')}\right), \mathcal{R}_d\right), \quad (8)$$

$$\text{where } \Phi_n^{(d,s)} = f^{(d)}(\mathbf{X}_n^s; \mathcal{F}) \text{ and } \Phi_q^{*(d,s')} = f^{(d)}(\mathbf{X}_q^{*s'}; \mathcal{F}),$$

with the following MSE loss:

$$\arg \min_{\mathcal{F}, \mathcal{R}_1, \dots, \mathcal{R}_D} L_R, \quad \text{where } L_R = \quad (9)$$

$$\mathbb{E}_{(\mathcal{W}_1, \dots, \mathcal{W}_L, q) \sim \mathcal{E}} \sum_{l \in \mathcal{J}_L} \sum_{d \in \mathcal{J}_D} \sum_{s \in \mathcal{S}} \sum_{s' \in \mathcal{S}} \frac{1}{ss'} \left( \zeta_{lq}^{(d,ss')} - \delta(c_l - c_q^*) \right)^2.$$

Such a basic formulation outperforms our earlier formulations. However, the relation network in Eq. (8) and the loss in Eq. (9) can be modified to form a better strategy utilizing the abstraction level and scale matching steps, as detailed next.

**Feature Matching (FM).** Although MISo can extract feature vectors at various spatial scales and levels of visual abstraction, not all scales and visual abstraction levels have the same importance. Figure 5 shows that the features across different levels may contain foreground, context or even background information. In order to control the respective contributions of each scale and level of feature abstraction, we introduce a so-called Feature Matching. The FM step acts as an adaptive switch or weight for every branch of the relation learner.

Moreover, FM can be applied at the intra- or inter-level. Figure 4 (a) shows that FM can be applied within the single-

level scale-wise features. Such a strategy is called intra-level matching as exclusive base learners are trained to make predictions at each respective level. Alternatively, one can choose to apply FM over multi-level representations, as shown in Figure 4 (b). Such a strategy employs a shared base learner to make predictions over all available pairs.

For intra- and inter-matching, we investigate four types of matching: Cosine Matching (CM), Gate Module (GM), Optimal Transport (OT) and GRaph matching (GR). Let us take the intra-level matching scheme as example.

Let  $\boldsymbol{\psi}_n^{(d,s)} \equiv (\Psi_n^{(d,s)})_{(\cdot)}$  and  $\boldsymbol{\psi}_q^{*(d,s')} \equiv (\Psi_q^{*(d,s')})_{(\cdot)}$  be pooled (as in Eq. (12) but without the concatenation step) support and query descriptors, vectorized by the operator  $(\cdot)$ .

**Cosine Matching (CM)** simply reweights scale-wise feature pairs via the cosine similarity  $\alpha_{nq}^{(d,ss')} = \langle \boldsymbol{\psi}_n^{(d,s)}, \boldsymbol{\psi}_q^{*(d,s')} \rangle$ .

**Gate Module (GM)** in Fig. 3 learns to assign an attention score for each pair based on a convolutional network  $g(\cdot)$  so that  $\alpha_{nq}^{(d,ss')} = g(\boldsymbol{\psi}_n^{(d,s)}) \cdot g(\boldsymbol{\psi}_q^{*(d,s')})$ . For CM and GM, the updated relation score is defined as follows:

$$\zeta_{nq}^{(d)} = \alpha_{nq}^{(d,ss')} r(\boldsymbol{\psi}_n^{(d,s)}, \boldsymbol{\psi}_q^{*(d,s')}; \mathcal{R}_d). \quad (13)$$

Subsequently, we form the following MSE loss:

$$\arg \min_{\mathcal{F}, \mathcal{R}_1, \dots, \mathcal{R}_D} L_R = \quad (14)$$

$$\text{where } L_R = \mathbb{E}_{(\mathcal{W}_1, \dots, \mathcal{W}_L, q) \sim \mathcal{E}} \sum_{l \in \mathcal{J}_L} \sum_{n \in \mathcal{W}_l} \sum_{d \in \mathcal{J}_D} \left( \zeta_{nq}^{(d)} - \delta(c_l - c_q^*) \right)^2,$$

where the label-related symbols are defined as for Eq. (3).

**Optimal Transport (OT).** DeepEMD [96] transports the support location-wise representations to match the query location-wise representations (location-wise matching). In contrast, we propose a strategy complementary to design of DeepEMD. We solve a linear program to transport the support intra-level

scale-wise representations into the query intra-level scale-wise representations. We obtain the dominant matching pattern of spatial scales at the given abstraction levels by:

$$\zeta_{nq}'^{(d)} = 1 - \min_{\omega_{nq}^{(d)} \geq 0} \sum_{s,s'} \omega_{nq}^{(d,ss')} \alpha_{nq}^{(d,ss')}, \quad (15)$$

$$\text{s.t. } \sum_{s'} \omega_{nq}^{(d,ss')} = \Omega_n^{(d,s)}, \quad \sum_s \omega_{nq}^{(d,ss')} = \Omega_q^{*(d,s')},$$

$$\text{where } \alpha_{nq}^{(d,ss')} = \langle \Psi_n^{(d,s)}, \Psi_q^{*(d,s')} \rangle,$$

and  $\Omega_n^{(d,s)} = \max(0, \langle \Psi_n^{(d,s)}, \frac{1}{N_s} \sum_{s'=1}^S \Psi_q^{*(d,s')} \rangle)$  and  $\Omega_q^{*(d,s')} = \max(0, \langle \Psi_q^{*(d,s')}, \frac{1}{N_s} \sum_{s=1}^S \Psi_n^{(d,s)} \rangle)$  constraint weights  $\omega_{nq}^{(d,ss')}$ . Subsequently, we apply the loss in Eq. (15).

**GRaph matching (GR)** strategy is based on a Graph Neural Network (GNN), which learns correlations between support and query samples at different levels of abstraction and scales. To implement GR, we form an adjacency matrix  $\alpha_{nq}^{(d)} \in \mathbb{R}^{2S \times 2S}$  representing a weighted undirected graph capturing scales of the support-query pair for the abstraction level  $d$ . Following the standard GNN notation, we have  $\mathbf{H}_{nq}^{(d,l'+1)} = \sigma(\alpha_{nq}^{(d)} \mathbf{H}_{nq}^{(d,l')} \mathbf{W}^{(l')})$ , where  $\sigma(\cdot)$  is a non-linearity and  $l'$  refers to the GNN layer index. The node information matrix is given by  $\mathbf{H}_{nq}^{(d,1)} \equiv \left[ \left[ \Psi_n^{(d,s)} \right]_{s \in \mathcal{S}_S}^T; 1 \left[ \Psi_q^{*(d,s')} \right]_{s' \in \mathcal{S}_S}^T \right]$ , and  $\mathbf{W}^{(l')}$  are filters of GNN. The adjacency matrix  $\alpha$  is defined as:

$$\alpha_{nq}^{(d)} = \begin{bmatrix} \left[ \langle \Psi_n^{(d,s)}, \Psi_n^{(d,s')} \rangle \cdot e^{-\frac{(s-s')^2}{2\sigma^2}} \right]_{\substack{s \in \mathcal{S}_S \\ s' \in \mathcal{S}_S}} & \left[ \langle \Psi_n^{(d,s)}, \Psi_q^{*(d,s')} \rangle \cdot e^{-\frac{(s-s')^2}{2\sigma^2}} \right]_{\substack{s \in \mathcal{S}_S \\ s' \in \mathcal{S}_S}} \\ \left[ \langle \Psi_q^{*(d,s')}, \Psi_n^{(d,s)} \rangle \cdot e^{-\frac{(s-s')^2}{2\sigma^2}} \right]_{\substack{s \in \mathcal{S}_S \\ s' \in \mathcal{S}_S}} & \left[ \langle \Psi_q^{*(d,s')}, \Psi_q^{*(d,s')} \rangle \cdot e^{-\frac{(s-s')^2}{2\sigma^2}} \right]_{\substack{s \in \mathcal{S}_S \\ s' \in \mathcal{S}_S}} \end{bmatrix}, \quad (16)$$

where the dot product  $\langle \cdot, \cdot \rangle$  captures the visual similarity between representations at scales  $s, s' \in \mathcal{S}_S$ , and  $e^{-\frac{(s-s')^2}{2\sigma^2}}$  is the Radial Basis Function (RBF) similarity prior w.r.t. scales  $s$  and  $s'$ . Moreover,  $\sigma = \frac{1}{3}(S-1)$  ensures that for the maximum difference of scales equal  $S-1$ , the RBF kernel decays by 90% of its maximum value of one.

Subsequently, we apply a fully-connected layer to  $\mathbf{H}^{(d,L')}$ , where the last layer  $L' = 3$ :

$$\zeta_{nq}'^{(d)} = \text{MLP} \left( \mathbf{H}_{nq}^{(d,L')} \right), \quad (17)$$

and then  $\zeta_{nq}'^{(d)}$  can be substituted into Eq. (15).

**Visual Abstraction Level and Scale Discriminator.** Self-supervised learning has become a mainstream tool in devising robust representations. Below we propose to employ a self-supervised Visual Abstraction Level and Scale Discriminator, called VALSD, whose role is to learn to predict the level of abstraction and the spatial scale indexes by observing the autocorrelation matrices of a given branch. Such a design is consistent with the idea of employing a simple pretext task. Self-supervised learning encourages the network to preserve additional information about images, leading to highly discriminative representations.

The VALSD unit is indicated in Figure 1. We proceed by simply taking second-order representations  $\Psi_n^{(d,s)}$  and  $\Psi_q^{*(d,s)}$  for each level of abstraction  $d \in \mathcal{S}_D$  and a spatial scale  $s \in \mathcal{S}_S$ , where  $(d,s)$  indexes serve as labels for the pretext task. We employ the softmax cross-entropy classifier on  $\Psi_n^{(d,s)}$  and

$\Psi_q^{*(d,s)}$  with the goal of predicting the joint abstraction-scale label  $d \cdot S + s$ , which ranges from 1 to 9 for  $S=3$  and three spatial scales.

## D. Unsupervised Pipeline

For completeness, below we introduce an unsupervised FSL pipeline which does not rely on any class-wise training annotations. Inspired by self-supervised learning, we apply extensive augmentations to available training images (or videos) to form the so-called positive set, and we label these instances as similar. The above step promotes FEN to learn invariance to augmentations in the embedding space.

Specifically, given two image inputs  $\mathbf{X}$  and  $\mathbf{Y}$ , we first apply random augmentations on these images *e.g.*, rotation, flip, resized crop and the color jitter via operator  $\text{Aug}(\cdot)$  which samples these transformations according to a uniform distribution. We obtain a set of  $M$  augmented images:

$$\widehat{\mathbf{X}}_n \sim \text{Aug}(\mathbf{X}), \quad \widehat{\mathbf{Y}}_q \sim \text{Aug}(\mathbf{Y}), \quad n, q \in \mathcal{S}_M. \quad (18)$$

Subsequently, we pass the augmented images to the feature encoder  $f$  and obtain their embeddings. Equations below assume  $D$  levels of feature abstraction but using a single level may be achieved by dropping the superscript  $(d)$  in what follows. For the augmented samples of  $\mathbf{X}$ , we form relation descriptors which represent positive pairs (similar instances). For the augmented samples of  $\mathbf{Y}$ , we repeat the above step to also form positive pairs. We then form exhaustively the relation descriptors between the augmented samples of  $\mathbf{X}$  and  $\mathbf{Y}$  which represent negative pairs (dissimilar instances). Finally, we obtain relation predictions  $\zeta^{(d)}, \zeta^{*(d)} \in \mathbb{R}^{M \times M}$  from the relation network  $r(\cdot)$  for the augmented samples of  $\mathbf{X}$  and  $\mathbf{Y}$ , respectively. We also obtain the relation predictions  $\zeta'^{(d)} \in \mathbb{R}^{M \times M}$  evaluated between the augmented samples of  $\mathbf{X}$  and  $\mathbf{Y}$ . The above steps are realized by:

$$\begin{aligned} \Phi_n^{(d)} &= f^{(d)}(\widehat{\mathbf{X}}_n; \mathcal{F}), \quad \Phi_q^{*(d)} = f^{(d)}(\widehat{\mathbf{Y}}_q; \mathcal{F}), \quad n, q, n', q' \in \mathcal{S}_M, \quad d \in \mathcal{S}_D, \\ \zeta_{nn'}^{(d)} &= r \left( \vartheta \left( \Phi_n^{(d)}, \Phi_{n'}^{(d)} \right); \mathcal{R}_d \right), \\ \zeta_{nq}^{(d)} &= r \left( \vartheta \left( \Phi_n^{(d)}, \Phi_q^{*(d)} \right); \mathcal{R}_d \right), \\ \zeta_{qq'}^{*(d)} &= r \left( \vartheta \left( \Phi_q^{*(d)}, \Phi_{q'}^{*(d)} \right); \mathcal{R}_d \right). \end{aligned} \quad (19)$$

Finally, we minimize the contrastive loss  $L_{uns}$  w.r.t.  $\mathcal{F}$  and  $\mathcal{R}$  in order to push closer the positive embedding pairs of the augmented samples generated from the same image ( $\mathbf{X}$  followed by  $\mathbf{Y}$ ) and push apart the negative pairs of embeddings of the augmented samples generated from  $\mathbf{X}$  and  $\mathbf{Y}$  (two different images):

$$\arg \min_{\mathcal{F}, \mathcal{R}_1, \dots, \mathcal{R}_D} \mathbb{E}_{(\widehat{\mathbf{X}}_n, \widehat{\mathbf{Y}}_q)_{n, q \in \mathcal{S}_M}} \mathbb{E}_{d \in \mathcal{S}_D} \left( \|\zeta^{(d)} - 1\|_F^2 + \|\zeta^{*(d)} - 1\|_F^2 + \|\zeta'^{(d)}\|_F^2 \right),$$

where  $(\mathbf{X}, \mathbf{Y}) \sim \mathcal{E}_{uns}$  and  $(\widehat{\mathbf{X}}_n, \widehat{\mathbf{Y}}_q) \sim \text{Aug}(\mathbf{X}) \times \text{Aug}(\mathbf{Y})$ .

(20)

During the inference step, we simply apply Eq. (6).



**TABLE II:** Evaluations on the Omniglot dataset.

Model	Fine Tune	5-way accuracy		20-way accuracy	
		1-shot	5-shot	1-shot	5-shot
<i>Conv. Siamese Nets</i> [32]	N	96.7	98.4	88.0	96.5
<i>Conv. Siamese Nets</i> [32]	Y	97.3	98.4	88.1	97.0
<i>Matching Net</i> [84]	N	98.1	98.9	93.8	98.5
<i>Prototypical Net</i> [73]	N	99.8	99.7	96.0	98.9
<i>MAML</i> [13]	Y	98.7	99.9	95.8	98.9
<i>Relation Net</i> [78]	N	99.6	99.8	97.6	99.1
<i>SoSN+PN</i> - - -	N	99.8	99.9	98.3	99.4
<i>MISo+PN</i>	N	<b>99.9</b>	<b>99.9</b>	<b>98.7</b>	<b>99.7</b>

## V. EXPERIMENTS

Below we demonstrate the usefulness of our approach by evaluating it on the Omniglot [45], *mini-ImageNet* [84] and *tiered-ImageNet* [62] datasets, a recently proposed Open MIC dataset [36], fine-grained Flower102 [54], CUB-200 [85] and Food-101 [3] datasets, and action recognition datasets such as HMDB51 [44], UCF101 [75] and *mini-MIT* [75]. We evaluate the performance of SoSN and MISo in both supervised and unsupervised settings to demonstrate their superior performance compared to first-order representations in few-shot learning. We train our network with the Adam solver. The layer configurations of our SoSN model are shown in Figure 3. The results are compared against several state-of-the-art methods in one- and few-shot learning.

### A. Datasets

Below we describe our setup, as well as the category recognition, fine-grained and action recognition datasets.

**Omniglot** [45] consists of 1623 characters from 50 alphabets. Samples in each class are drawn by 20 different people. The dataset is split into 1200 classes for training and 423 classes for testing. All images are resized to  $28 \times 28$  pixels.

***mini-ImageNet*** [84] consists of 60000 RGB images from 100 classes, each class containing 600 samples. We follow the standard protocol [84] and use 80 classes for training (16 classes selected for validation) and remaining 20 classes for testing. We use images of  $84 \times 84$  pixels.

***tiered-ImageNet*** [62] consists of 608 classes from ImageNet. We follow the protocol with 351 base classes, 96 validation classes and 160 novel test classes.

**Open MIC** stands for the Open Museum Identification Challenge (Open MIC) [36], a recent dataset with photos of various exhibits *e.g.*, paintings, timepieces, sculptures, glassware, relics, science exhibits, natural history pieces, ceramics, pottery, tools and indigenous crafts, captured within 10 museum exhibition spaces according to which this dataset is divided into 10 sub-problems. In total, Open MIC has 866 diverse classes and 1–20 images per class. The within-class images undergo various geometric and photometric distortions as the data was captured with wearable cameras. This makes Open MIC a perfect candidate for testing one-shot learning algorithms. We combine (*shn+hon+clv*), (*clk+gls+scl*), (*sci+nat*) and (*shx+rlc*) into sub-problems *p1*, ..., *p4*. We form 12 possible pairs in which sub-problem *x* is used for training and sub-problem *y* is used for testing ( $x \rightarrow y$ ).

**Caltech-UCSD-Birds 200-2011 (CUB Birds)** [85] has 11788 images of 200 bird species. We follow the splits from [24],

that is, 130 classes are selected for training, 20 classes for validation and the remaining 50 categories for testing.

**Stanford Dogs** [43] has 17150 instances of 120 dogs classes where 70 classes are used for training, 20 classes for validation and the remaining 30 classes for testing, which is consistent with the protocol in [24].

**Stanford Cars** [28] dataset has 16190 samples of 196 car categories. Following the protocol in [24], we use the 130/17/49 class splits for training, validation and testing, respectively.

**HMDB51** [44], an action recognition dataset, contains 6849 clips divided into 51 action categories, each with a minimum of 101 clips. Following the protocol in [100], 31 classes are selected for training, 10 classes are used for validating and the remaining 10 classes are used for testing.

**UCF101** [75] contains action videos collected from YouTube. It has 13320 video clips and 101 action classes. Following the protocol in [100], we pick 70 classes for training, 10 classes for validation and the remaining 21 classes for testing.

***mini-MIT*** [52] is a subset of the newly proposed large-scale Moments in Time dataset. This mini version contains 200 classes with 550 videos per class. Following the protocol in [100], we select 120 classes for training, 40 classes for validation and the rest 40 classes for testing.

### B. Experimental Setup

For the Omniglot dataset, we follow the setup in [78]. For *mini-ImageNet*, we use the 5-way 1-shot and 5-way 5-shot protocols. For every training and testing episodes, we randomly select 5 and 3 query samples per class, respectively. We compute an average over 600 episodes to obtain results. We use the initial learning rate of  $1e-3$  and train the model with 200000 episodes. For *tiered-ImageNet*, we follow the settings used for the *mini-ImageNet* dataset. For Open MIC, we mean-center images per sub-problem. We use the initial learning rate of  $1e-4$  and train the network with 15000 episodes. For the fine-grained classification datasets, we evaluate our models on the 5-way 1-shot and 5-way 5-shot protocols. The numbers of support and query samples in each episode are the same as in the *mini-ImageNet* setting. We use the initial learning rate of  $1e-3$  and train the model with 200000 episodes. For the action recognition datasets, we randomly sample 50 frames per video along the temporal mode. We resize video frames to  $84 \times 84$  pixels, which results in a lightweight model. We evaluate our algorithm on the 5-way 1-shot and 5-way 5-shot protocols on the three datasets detailed earlier. We adopt the hyper-parameter configuration used on the *mini-ImageNet* dataset.

### C. Evaluation Results

Below we evaluate SoSN and its multi-level extension MISo, and we compare them with state-of-the-art methods on datasets introduced above.

**Omniglot.** Table II shows rather saturated results. We consider experiments on the Omniglot dataset as a sanity check to validate the performance of SoSN in the best default setting, that is, using the relationship descriptor from Eq. (12) and

**TABLE III:** Evaluations on the *mini*-ImageNet dataset (5-way accuracy). Asterisk ‘\*’ highlights that we converted the supervised Prototypical Net and the supervised Relation Net into the unsupervised contrastive pipelines, U-Prototypical Net and U-Relation Net, using the same mechanism (described in Section IV-D) as the one applied for U-SoSN and U-MISo.

Model		Backbone	1-shot	5-shot
Supervised Pipelines				
<i>Prototypical Net</i>	[73]	Conv-4	49.42 ± 0.78	68.20 ± 0.66
<i>MAML</i>	[13]	Conv-4	48.70 ± 1.84	63.11 ± 0.92
<i>Relation Net</i>	[78]	Conv-4	50.44 ± 0.82	65.32 ± 0.70
<i>LwoF</i>	[15]	WRN	56.20 ± 0.86	72.81 ± 0.62
<i>GNN</i>	[67]	Conv-4	50.30	66.40
<i>Reptile</i>	[53]	Conv-4	49.97 ± 0.32	65.99 ± 0.58
<i>Saliency Net</i>	[99]	Conv-4	57.45 ± 0.86	72.01 ± 0.75
<i>MAML++</i>	[1]	Conv-4	52.15 ± 0.26	68.32 ± 0.44
<i>TPN</i>	[50]	Conv-4	55.51	69.86
<i>Boosting</i>	[14]	Conv-4	53.63 ± 0.43	71.70 ± 0.36
<i>TAML</i>	[25]	Conv-4	51.77 ± 1.86	65.60 ± 0.93
<i>KTN</i>	[56]	Conv-4	54.61 ± 0.80	71.21 ± 0.66
<i>ArL</i>	[98]	Conv-4	57.48 ± 0.65	72.64 ± 0.45
<i>TADAM</i>	[55]	ResNet-12	58.50 ± 0.30	76.70 ± 0.30
<i>Variational FSL</i>	[95]	ResNet-12	61.23 ± 0.26	77.69 ± 0.17
<i>DeepEMD</i>	[96]	ResNet-12	65.91 ± 0.82	82.41 ± 0.56
<i>MetaOptNet</i>	[46]	ResNet-18	62.64 ± 0.61	78.63 ± 0.46
<i>PN + SSL</i>	[76]	ResNet-18	58.40	76.60
<i>SimpleShot</i>	[89]	ResNet-18	63.10 ± 0.20	79.92 ± 0.14
<i>FLAT</i>	[94]	WRN-28-10	59.88 ± 0.83	77.14 ± 0.59
$\bar{SoSN}(\otimes + \bar{F}) + \bar{PN}$	Eq. (10)	Conv-4	50.57 ± 0.84	65.91 ± 0.71
<i>SoSN</i> ( $\otimes$ ) (no PN)	Eq. (12)	Conv-4	50.88 ± 0.85	66.71 ± 0.67
<i>SoSN</i> ( $\otimes + R$ ) + PN	Eq. (11)	Conv-4	52.96 ± 0.83	68.58 ± 0.70
<i>SoSN</i> ( $\otimes$ ) + PN	Eq. (12)	Conv-4	52.96 ± 0.83	68.63 ± 0.68
<i>MISo</i> ( $\otimes$ ) + PN	Eq. (12)	Conv-4	<b>58.03 ± 0.80</b>	<b>73.06 ± 0.72</b>
$\bar{SoSN}(\otimes) + \bar{PN}$	Eq. (12)	ResNet-12	58.26 ± 0.87	73.20 ± 0.68
<i>MISo</i> ( $\otimes$ ) + PN	Eq. (12)	ResNet-12	<b>66.08 ± 0.85</b>	<b>82.32 ± 0.66</b>
<i>MISo</i> ( $\otimes$ ) + PN	Eq. (12)	ResNet-18	<b>66.79 ± 0.86</b>	<b>83.41 ± 0.67</b>
Unsupervised Pipelines				
<i>Pixel (Cosine)</i>		-	23.00	26.60
<i>BiGAN</i> ( $k_m$ )	[10]	-	25.56	31.10
<i>BiGAN</i> (cluster match)	[10]	-	24.63	29.49
<i>DeepCluster</i> ( $k_m$ )	[6]	-	28.90	42.25
<i>DeepCluster</i> (cluster match)	[6]	-	22.20	23.50
<i>U-Prototypical Net</i> *	[73]	Conv-4	35.85	48.01
<i>U-Relation Net</i> *	[78]	Conv-4	35.14	44.10
<i>UMTRA</i>	[27]	Conv-4	39.91	50.70
<i>CACTUs</i>	[21]	Conv-4	39.94	54.01
$\bar{U-SoSN}(\otimes) + \bar{PN}$		Conv-4	37.94	50.95
<i>U-MISo</i> + PN		Conv-4	<b>41.09</b>	<b>55.38</b>

**TABLE IV:** Evaluations on the *tiered*-ImageNet dataset (5-way accuracy) with the Conv-4 backbone.

Model		1-shot	5-shot
<i>Incremental</i>	[61]	51.12 ± 0.45	66.40 ± 0.36
<i>Soft k-means</i>	[62]	52.39 ± 0.44	69.88 ± 0.20
<i>MAML</i>	[13]	51.67 ± 1.81	70.30 ± 0.08
<i>Reptile</i>	[53]	48.97 ± 0.21	66.47 ± 0.21
<i>Prototypical Net</i>	[73]	53.31 ± 0.89	72.69 ± 0.74
<i>Relation Net</i>	[78]	54.48 ± 0.93	71.32 ± 0.78
<i>TPN</i>	[50]	57.41 ± 0.94	71.55 ± 0.74
$\bar{SoSN}$		58.62 ± 0.92	75.19 ± 0.79
<i>MISo</i>		<b>61.97 ± 0.91</b>	<b>78.83 ± 0.77</b>
Unsupervised Pipelines			
<i>U-Prototypical Net</i>	[73]	37.52 ± 0.93	51.03 ± 0.84
<i>U-Relation Net</i>	[78]	37.23 ± 0.94	49.54 ± 0.83
$\bar{U-SoSN}$		41.59 ± 0.92	55.81 ± 0.76
<i>U-MISo</i>		<b>43.01 ± 0.91</b>	<b>57.53 ± 0.74</b>

Power Normalization from Proposition 3. We note that the basic multi-level multi-scale variant of MISo based on Eq. (9) outperforms SoSN.

**mini-ImageNet.** Table III demonstrates that our method outperforms other approaches on both 1- and 5-shot evaluation protocols. Firstly, we note that comparisons between various relation descriptors with/without PN are included and discussed as ablation studies in Section V-D.

For the image size of  $84 \times 84$  and the 5-way 1-shot experiment, our best single-level SoSN model achieves  $\sim 2.5\%$  higher accuracy than Relation Net [78]. Our best single-level SoSN also outperforms Prototypical Net by  $\sim 3.5\%$  accuracy on the 5-way 1-shot protocol. Not shown in the table are results for SoSN trained with images of  $224 \times 224$  pixels, in which case the accuracy scores on both protocols increase by 5.45% and 4.33%, respectively. Such an accuracy gain demonstrates that SoSN benefits from large image sizes as second-order matrices are of higher rank for higher image resolutions due to the higher spatial resolution of feature maps compared with the low-resolution counterparts. Our similarity learning network works with variable resolutions of input images because SoSN operates on matrices whose size depends only on the number of output channels of encoding network.

**TABLE V:** Evaluations on the fine-grained classification datasets (5-way accuracy) with the Conv-4 backbone.

Model		CUB Birds		Stanford Dogs		Stanford Cars	
		1-shot	5-shot	1-shot	5-shot	1-shot	5-shot
<i>Matching Net</i>	[84]	45.30 ± 1.03	59.50 ± 1.01	35.80 ± 0.99	47.50 ± 1.03	34.80 ± 0.98	44.70 ± 1.03
<i>MAML</i>	[13]	58.13 ± 0.36	71.51 ± 0.30	44.84 ± 0.31	58.61 ± 0.30	47.25 ± 0.30	61.11 ± 0.29
<i>Proto. Net</i>	[73]	37.36 ± 1.00	45.28 ± 1.03	37.59 ± 1.00	48.19 ± 1.03	40.90 ± 1.01	52.93 ± 1.03
<i>Relation Net</i>	[78]	58.99 ± 0.52	71.20 ± 0.40	43.29 ± 0.46	55.15 ± 0.39	47.79 ± 0.49	60.60 ± 0.41
<i>LRPABN</i>	[24]	63.63 ± 0.77	76.06 ± 0.58	45.72 ± 0.75	60.94 ± 0.66	60.28 ± 0.76	73.29 ± 0.63
<i>MattML</i>	[106]	66.29 ± 0.56	80.34 ± 0.30	54.84 ± 0.53	71.34 ± 0.38	66.11 ± 0.54	82.80 ± 0.28
<i>SoSN</i>	[97]	64.56 ± 0.91	77.82 ± 0.57	48.21 ± 0.72	63.15 ± 0.67	62.88 ± 0.72	76.10 ± 0.58
<i>MISo</i>		<b>68.21 ± 0.78</b>	<b>82.18 ± 0.47</b>	<b>55.62 ± 0.58</b>	<b>71.98 ± 0.71</b>	<b>67.83 ± 0.63</b>	<b>84.98 ± 0.48</b>
<i>U-Proto. Net</i>	[78]	34.51 ± 0.53	56.32 ± 0.41	32.05 ± 0.49	43.96 ± 0.48	33.87 ± 0.57	48.20 ± 0.46
<i>U-Relation Net</i>	[78]	35.42 ± 0.55	57.96 ± 0.43	32.75 ± 0.49	44.37 ± 0.46	34.43 ± 0.54	48.71 ± 0.45
<i>U-SoSN</i>	[97]	43.14 ± 0.51	65.02 ± 0.43	41.56 ± 0.49	53.62 ± 0.47	40.31 ± 0.55	57.98 ± 0.43
<i>U-MISo</i>		<b>46.31 ± 0.53</b>	<b>68.67 ± 0.46</b>	<b>45.02 ± 0.48</b>	<b>56.89 ± 0.46</b>	<b>43.81 ± 0.56</b>	<b>61.13 ± 0.41</b>

**TABLE VI:** Evaluations on the action recognition benchmarks (5-way accuracy). To fairly compare our method with the prior works, we follow the same evaluation splits with [100]. For our baselines, we re-implement the Prototypical Net and the Relation Net both with the use of 3D convolutions.

Model		HMDB51		UCF101		mini-MIT		Kinetics	
		1-shot	5-shot	1-shot	5-shot	1-shot	5-shot	1-shot	5-shot
<i>C3D PN</i>	[73]	38.05 ± 0.97	53.15 ± 0.90	57.05 ± 1.02	78.25 ± 0.73	33.65 ± 1.01	45.1 ± 0.90	57.11	77.92
<i>C3D RN</i>	[78]	38.23 ± 0.97	53.17 ± 0.86	58.21 ± 1.02	78.35 ± 0.72	35.71 ± 1.02	47.32 ± 0.91	56.98	77.83
<i>C3D SoSN</i>	[97]	40.83 ± 0.96	55.18 ± 0.86	62.57 ± 1.05	81.51 ± 0.75	40.83 ± 0.99	52.16 ± 0.95	58.77	79.02
<i>CMN</i>	[105]	-	-	-	-	-	-	60.50	78.90
<i>ARN</i>	[100]	45.52 ± 0.96	58.96 ± 0.87	66.32 ± 0.99	83.12 ± 0.70	43.05 ± 0.97	56.71 ± 0.87	63.70	82.40
<i>C3D MISo</i>		<b>46.69 ± 0.93</b>	<b>60.31 ± 0.83</b>	<b>68.19 ± 0.95</b>	<b>87.11 ± 0.71</b>	<b>44.67 ± 0.95</b>	<b>58.68 ± 0.86</b>	<b>66.32</b>	<b>85.21</b>

**TABLE VII:** Evaluations on the Open MIC dataset (Protocol I) (5-way 1-shot accuracy).

Model		$p1 \rightarrow p2$	$p1 \rightarrow p3$	$p1 \rightarrow p4$	$p2 \rightarrow p1$	$p2 \rightarrow p3$	$p2 \rightarrow p4$	$p3 \rightarrow p1$	$p3 \rightarrow p2$	$p3 \rightarrow p4$	$p4 \rightarrow p1$	$p4 \rightarrow p2$	$p4 \rightarrow p3$
<i>Matching Net</i>	[84]	68.7	52.3	60.9	45.6	48.1	69.1	48.0	46.9	65.7	42.1	68.9	50.5
<i>MAML</i>	[13]	69.1	52.8	61.8	46.4	48.2	69.1	48.4	48.3	65.8	43.2	70.2	50.2
<i>Reptile</i>	[53]	69.2	52.5	62.2	47.1	48.8	69.3	48.5	48.7	66.1	43.6	70.1	50.3
<i>Proto. Net</i>	[73]	70.0	53.9	62.1	46.5	49.7	69.9	49.1	48.2	67.1	43.9	70.5	51.1
<i>Relation Net</i>	[78]	71.1	53.6	63.5	47.2	50.6	68.5	48.5	49.7	68.4	45.5	70.3	50.8
<i>SoSN</i>	[97]	81.4	65.2	75.1	60.3	62.1	77.7	61.5	82.0	78.0	59.0	80.8	62.5
<i>MISo</i>		<b>81.6</b>	<b>66.3</b>	<b>77.2</b>	<b>62.4</b>	<b>63.1</b>	<b>78.2</b>	<b>64.2</b>	<b>81.4</b>	<b>78.0</b>	<b>60.1</b>	<b>81.6</b>	<b>63.6</b>
<i>U-Relation Net</i>	[78]	67.1	48.1	62.5	41.2	45.3	58.0	50.1	57.5	53.8	46.9	66.1	43.3
<i>U-SoSN</i>	[97]	78.6	58.8	74.3	61.1	57.9	72.4	62.3	75.6	73.7	58.5	76.5	54.6
<i>U-MISo</i>		<b>80.9</b>	<b>61.5</b>	<b>76.3</b>	<b>62.0</b>	<b>60.3</b>	<b>75.1</b>	<b>64.1</b>	<b>77.9</b>	<b>76.2</b>	<b>59.9</b>	<b>79.1</b>	<b>58.2</b>

p1: shn+hon+clv, p2: clk+gls+scl, p3: sci+nat, p4: shx+rlc. Notation  $x \rightarrow y$  means training on exhibition  $x$  and testing on  $y$ .

Furthermore, our variant of MISo with the ResNet-12 backbone, based on the inter-level matching strategy of the multi-level multi-scale feature representations by the Gate Module, achieved a significant gain between 6% and 9% accuracy over SoSN. For unsupervised FSL, Table III shows that our U-SoSN and U-MISo significantly outperform other unsupervised baselines ('U-' stands for the unsupervised FSL setting) e.g., U-Relation Net and U-Prototypical Net. Compared to the U-SoSN model, the U-MISo model improves the top-1 accuracy by another 2% and 3% on the 1- and 5-shot protocols, respectively.

We discuss the ablations on MISo in Section V-D. Firstly, we discuss the results of the single-level SoSN model on more datasets. In the following tables, we drop '( $\otimes$ )+PN' from our notations but this particular relation descriptor with PN is the best performing variant, thus it is used across the remaining experiments.

**tiered-ImageNet.** Table IV shows the performance of our proposed methods on *tiered-ImageNet*. Our SoSN achieves  $\sim 4.1\%$  and  $3.9\%$  improvement in accuracy, compared with Relation Net for 1- and 5-shot protocols, respectively. More-

over, MISo with the Gate Module achieves  $\sim 7.0\%$  and  $3.9\%$  improvement in accuracy, compared with Relation Net for 1- and 5-shot protocols, respectively. The unsupervised variant, U-MISo, yields  $\sim 6\%$  and  $8\%$  gain in accuracy over U-Relation Net for 1- and 5-shot protocols, respectively. Our supervised and unsupervised FSL models outperform all other FSL approaches based on the Conv-4 backbone.

**Open MIC.** Table VII demonstrates that our single-level SoSN model outperforms the Relation Net [78] for all train/test sub-problems of Protocol I. For the 5- and 20-way protocols, Relation Net scores 55.45% and 31.58% accuracy, respectively. In contrast, our single-level SoSN scores 70.46% and 49.05% accuracy, respectively.

For the unsupervised pipelines, the U-SoSN and U-MISo models achieve very promising results on Open MIC considering no class-wise annotations were used during the training step. To demonstrate this point further, the performance of U-SoSN is better than that of the supervised Relation Net. The U-MISo model with the Gate Module further outperforms U-SoSN by up to  $\sim 3\%$  accuracy, which is close to the performance of the supervised SoSN model. Specifically, U-

**TABLE VIII:** Ablation study on *mini*-ImageNet w.r.t. different modules of our pipeline (5-way accuracy, the ‘Conv-4-64’ backbone, 4 stages and 3 scales, and OT matching were used.)

Baseline	SB	FM	VALSD	1-shot	5-shot
✓				55.93	71.05
✓	✓			57.28	72.01
✓	✓	✓		57.79	72.65
✓	✓	✓	✓	<b>58.03</b>	<b>73.06</b>

**TABLE IX:** Ablation study on *mini*-ImageNet w.r.t. the number of abstraction levels and spatial scales (1-shot/5-shot accuracy, FM and VALSD were not used).

		Levels		
		2	3	4
Scales	1	55.24/70.85	55.66/70.88	55.93/71.05
	2	55.95/70.77	56.19/71.13	56.63/71.72
	3	56.67/71.81	57.03/71.98	<b>57.28/72.01</b>

MISo outperformed supervised SoSN on 4 splits. The above experiment shows that the unsupervised framework is especially effective in the scenario if (i) the number of training samples from the base classes is limited, and (ii) the problem is closely related to the image retrieval rather than the pure object category recognition.

**Fine-grained FSL.** For the fine-grained datasets, our proposed models are evaluated on the CUB Birds [85], Stanford Dogs [28] and Cars [43] datasets given the 5-way 1-shot and 5-way 5-shot protocols. We follow the same training, validation and testing splits as provided in [24]. Table V demonstrates that our models outperform the baseline models such as Relation Net [78], LRPABN [24] and MattML [106]. For CUB Birds, our best MISo with FM (OT) achieves  $\sim 9.2\%$  and  $\sim 11.0\%$  improvements in accuracy (the 1- and 5-shot protocols, respectively) compared to the 1-st order Relation Net. For the Stanford Dogs and Cars datasets, the overall improvements of our MISo are more significant. To illustrate this point, MISo outperforms Relation Net by up to  $\sim 12.4\%$  and  $\sim 16.8\%$  accuracy on Stanford Dogs, and  $\sim 20.0\%$  and  $\sim 24.8\%$  on Stanford Cars (the 1- and 5-shot protocols, respectively). Furthermore, our unsupervised FSL variants, U-SoSN and U-MISo, attain even higher gains in accuracy which are often in the range of between 10% and 25% compared to U-Relation Net.

**Few-shot Action Recognition (FSAR).** We conclude our evaluations on FSL Action Recognition, denoted as FSAR for short. To this end, results are obtained on the HMDB51 [44], UCF101 [75] and *mini*-MIT [52] datasets. We follow the evaluation protocols in [100]. As every action clip may contains hundreds of frames, we resize all frames to  $84 \times 84$  pixels and downsample clips along the temporal mode to reduce the usage of the GPU memory and limit the computational footprint. Table VI shows that our MISo outperforms the C3D Relation Net, SoSN and CMN [105] models. These results are consistent with our evaluations on the category recognition and fine-grained datasets.

**TABLE X:** Ablation study on *mini*-ImageNet w.r.t. the choice of matching algorithm and mode on the *mini*-Imagenet dataset (1- and 5-shot accuracy). We used the ‘Conv-4-64’ backbone.

shot	Intra-level Matching				Inter-level Matching			
	CM	GM	OT	GR	CM	GM	OT	GR
1	57.49	57.83	<b>58.03</b>	57.79	56.87	57.72	57.91	56.91
5	72.21	72.58	<b>73.06</b>	72.49	71.59	72.43	72.36	71.77

#### D. Ablation Studies

Below we conduct ablations studies and provide discussions regarding several components of our pipeline.

**Relationship Descriptors and Power Normalization.** Firstly, Table III shows that the use of PN brings  $\sim 0.8\%$  gain in accuracy over not using it. Not included in the tables, similar were our observations on the Open MIC dataset. Given the simplicity of PN, we have included it in our evaluations unless stated otherwise.

Relationship descriptors from Table I are evaluated in Table III according to which the single-level SoSN( $\otimes$ ) model outperforms the single-level SoSN( $\otimes$ +F) and SoSN( $\otimes$ +R) models. We expect that averaging over  $Z$  support descriptors from  $Z$  support images, as in SoSN( $\otimes$ ), removes the uncertainty in few-shot statistics, whereas the outer-products of support/query datapoints still enjoy the benefit of spatially-wise large convolutional feature maps (which helps form the robust second-order statistics).

**Importance of Second-order Pooling.** Table IV (*tiered*-ImageNet) shows that Relation Net achieves 54.48% and 71.32 % accuracy on the 1- and 5-shot protocols, respectively. Relation Net can be considered identical with the SoSN model but it uses first-order pooling. In contrast, SoSN achieves 58.62 and 75.19 % accuracy (1- and 5-shot protocols, respectively). The gain in accuracy can be attributed to the fact that SoSN is equipped with second-order pooling.

Table III shows that on *mini*-ImageNet, Relation Net scores 50.44% and 65.32% accuracy on the 1- and 5-shot protocols, whereas SoSN scores 52.96% and 68.63% accuracy, respectively.

The similar trend can be observed on *mini*-ImageNet when aggregating over feature maps of images of  $256 \times 256$  pixels. In such a setting (not included in the tables as  $256 \times 256$  pixels resolution is not a part of standard FSL protocol), Relation Net yields 54.01% and 68.56% accuracy on the 1- and 5-shot protocols. In contrast, SoSN yields 57.74% and 71.08% accuracy, respectively.

SoP represents features of each image as second-order statistics which are invariant to the spatial order of features in feature maps, and the spatial size of these feature maps. Second-order statistics are also richer than first-order statistics, as indicated by gains in accuracy attained by SoSN in comparison with Relation Net. SoP is the most beneficial when feature representations provide many feature vectors for aggregation *e.g.*,  $N \geq d$ . In such a case, the autocorrelation matrices may be of full rank (rank- $d$ ), thus capturing more statistical information in comparison to the first-order prototypes (equivalent of the rank-1 statistic).

**MISo, SB, FM and VALSD.** Table III demonstrates on *mini*-ImageNet that our MISo outperforms SoSN and a larger number of prior works. The performance on the 5-way 1-shot and 5-way 5-shot protocols achieves the peak gain of  $\sim 6.0\%$  in accuracy given 4 encoding levels and the Optimal Transport matching step, compared to the best single-level SoSN model.

Table VIII shows that adding our Scale-wise Boosting (SB), the Feature Matching (FM) and the Visual Abstraction Level and Scale Discriminator (VALSD) yields around 2% gain in accuracy over the baseline model. For the SB+FM case, we mean that the advanced abstraction level and spatial scale matching strategy is used, thus the loss in Eq. (15) is used for SB+FM, whereas the loss in Eq. (9) is used for SB alone.

Table IX shows that using four level of visual abstraction and three spatial scales is the best, which is consistent with our claim that the levels of visual abstraction and spatial scales need to be taken into account in few-shot learning.

Table X shows that the Intra-level Matching strategy is overall better than the Inter-level Matching strategy. This is consistent with our expectations as the levels of visual abstraction and spatial scales are quite complementary. Therefore, matching spatial scales irrespective of abstraction levels is a meaningful strategy. Finally, the Gate Module and the Optimal Transport are two best performing strategies, followed by the GRaph matching (GR) strategy and the Cosine Matching (CM) strategy. We suspect that GR was somewhat suboptimal due to the small-size dense adjacency matrix in our problem rather than the large scale sparse adjacency matrix which would normally capture a complex topology of some large graph (node classification, *etc.*). OT performed robust matching as it is designed to find an optimal transportation plan between different levels of abstraction and spatial scales of support-query pairs. Nonetheless, GM appears to provide the best matching trade-off, that is, GM is almost as good as OT in terms of accuracy, and it is faster than OT in terms of computational complexity (*i.e.*, there is no need to solve any linear programs). Finally, Figure 5 shows the visualization of multiple levels of feature abstraction in our FEN. Across all visualizations and their Gate Module scores (GM), the coarse-to-fine levels of feature abstraction appear to be complementary with each other.

## VI. CONCLUSIONS

We have presented the end-to-end trainable SoSN and MISo models for supervised and unsupervised few-shot learning. With the use of multiple levels of feature abstractions, multiple spatial scales, the Gate Module and the Visual Abstraction Level and Scale Discriminator, we have shown how to learn efficiently the similarity between the support-query pairs captured by the relation descriptors. We have investigated how to capture relations between the query and support matrices, and how to produce multiple complementary levels of feature information. We have also investigated several strategies for the level of abstraction and spatial scale matching to showcase the importance of decomposing the support-query pairs into multiple spatial scales at multiple levels of feature abstraction. MISo demonstrates consistent large gains in accuracy across

all benchmarks for both supervised and unsupervised learning. Given the simplicity of our approach, we believe that the SoSN and MISo models are interesting propositions that can serve as a starting point in designing more elaborate FSL approaches.

## REFERENCES

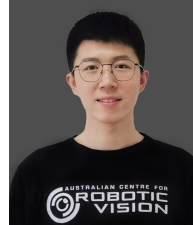
- [1] Antreas Antoniou, Harrison Edwards, and Amos Storkey. How to train your maml. In *International Conference on Learning Representations (ICLR)*, 2019. 2, 10
- [2] Evgeniy Bart and Shimon Ullman. Cross-generalization: Learning novel classes from a single example by feature replacement. In *2005 IEEE Computer Society Conference on Computer Vision and Pattern Recognition (CVPR'05)*, volume 1, pages 672–679. IEEE, 2005. 2
- [3] Lukas Bossard, Matthieu Guillaumin, and Luc Van Gool. Food-101 – mining discriminative components with random forests. In *European Conference on Computer Vision*, 2014. 9
- [4] Y Boureau, Jean Ponce, and Yann LeCun. A theoretical analysis of feature pooling in vision algorithms. In *Proc. International Conference on Machine Learning (ICML'10)*, volume 28, 2010. 3
- [5] Y-Lan Boureau, Francis Bach, Yann LeCun, and Jean Ponce. Learning mid-level features for recognition. In *2010 IEEE computer society conference on computer vision and pattern recognition*, pages 2559–2566. IEEE, 2010. 3
- [6] Mathilde Caron, Piotr Bojanowski, Armand Joulin, and Matthijs Douze. Deep clustering for unsupervised learning of visual features. In *Proceedings of the European Conference on Computer Vision (ECCV)*, pages 132–149, 2018. 10
- [7] Joao Carreira, Rui Caseiro, Jorge Batista, and Cristian Sminchisescu. Semantic segmentation with second-order pooling. In *European Conference on Computer Vision*, pages 430–443. Springer, 2012. 1, 3
- [8] Qiang Chen, Meng Wang, Zhongyang Huang, Yang Hua, Zheng Song, and Shuicheng Yan. Videopuzzle: Descriptive one-shot video composition. *IEEE Transactions on Multimedia*, 15(3):521–534, 2013. 3
- [9] Ting Chen, Simon Kornblith, Mohammad Norouzi, and Geoffrey Hinton. A simple framework for contrastive learning of visual representations. In *International conference on machine learning*, pages 1597–1607. PMLR, 2020. 1
- [10] Jeff Donahue, Philipp Krähenbühl, and Trevor Darrell. Adversarial feature learning. *arXiv preprint arXiv:1605.09782*, 2016. 10
- [11] Li Fei-Fei, Rob Fergus, and Pietro Perona. One-shot learning of object categories. *IEEE transactions on pattern analysis and machine intelligence*, 28(4):594–611, 2006. 2
- [12] Michael Fink. Object classification from a single example utilizing class relevance metrics. *NIPS*, pages 449–456, 2005. 2
- [13] Chelsea Finn, Pieter Abbeel, and Sergey Levine. Model-agnostic meta-learning for fast adaptation of deep networks. In *ICML*, pages 1126–1135, 2017. 2, 9, 10, 11
- [14] Spyros Gidaris, Andrei Bursuc, Nikos Komodakis, Patrick Pérez, and Matthieu Cord. Boosting few-shot visual learning with self-supervision. In *Proceedings of the IEEE/CVF International Conference on Computer Vision*, pages 8059–8068, 2019. 1, 2, 10
- [15] Spyros Gidaris and Nikos Komodakis. Dynamic few-shot visual learning without forgetting. In *Proceedings of the IEEE Conference on Computer Vision and Pattern Recognition*, pages 4367–4375, 2018. 10
- [16] Spyros Gidaris and Nikos Komodakis. Generating classification weights with gnn denoising autoencoders for few-shot learning. In *The IEEE Conference on Computer Vision and Pattern Recognition (CVPR)*, June 2019. 2
- [17] Kai Guo, Prakash Ishwar, and Janusz Konrad. Action recognition from video using feature covariance matrices. *IEEE Transactions on Image Processing*, 22(6):2479–2494, 2013. 1

- [18] Michelle Guo, Edward Chou, De-An Huang, Shuran Song, Serena Yeung, and Li Fei-Fei. Neural graph matching networks for fewshot 3d action recognition. In *Proceedings of the European Conference on Computer Vision (ECCV)*, pages 653–669, 2018. **3**
- [19] Mehrtash Harandi, Mathieu Salzmann, and Richard Hartley. Joint dimensionality reduction and metric learning: A geometric take. In *International Conference on Machine Learning*, pages 1404–1413. PMLR, 2017. **1**
- [20] Kaiming He, Haoqi Fan, Yuxin Wu, Saining Xie, and Ross Girshick. Momentum contrast for unsupervised visual representation learning. In *Proceedings of the IEEE/CVF Conference on Computer Vision and Pattern Recognition*, pages 9729–9738, 2020. **1**
- [21] Kyle Hsu, Sergey Levine, and Chelsea Finn. Unsupervised learning via meta-learning. In *International Conference on Learning Representations*, 2018. **10**
- [22] Guosheng Hu, Yang Hua, Yang Yuan, Zhihong Zhang, Zheng Lu, Sankha S Mukherjee, Timothy M Hospedales, Neil M Robertson, and Yongxin Yang. Attribute-enhanced face recognition with neural tensor fusion networks. In *Proceedings of the IEEE International Conference on Computer Vision*, pages 3744–3753, 2017. **1**
- [23] Yufan Hu, Junyu Gao, and Changsheng Xu. Learning dual-pooling graph neural networks for few-shot video classification. *IEEE Transactions on Multimedia*, 2020. **2, 3**
- [24] Huaxi Huang, Junjie Zhang, Jian Zhang, Jingsong Xu, and Qiang Wu. Low-rank pairwise alignment bilinear network for few-shot fine-grained image classification. *IEEE Transactions on Multimedia*, 2020. **2, 9, 11, 12**
- [25] Muhammad Abdullah Jamal and Guo-Jun Qi. Task agnostic meta-learning for few-shot learning. In *Proceedings of the IEEE/CVF Conference on Computer Vision and Pattern Recognition (CVPR)*, June 2019. **2, 10**
- [26] Hervé Jégou, Matthijs Douze, and Cordelia Schmid. On the burstiness of visual elements. In *2009 IEEE conference on computer vision and pattern recognition*, pages 1169–1176. IEEE, 2009. **3**
- [27] Siavash Khodadadeh, Ladislau Boloni, and Mubarak Shah. Unsupervised meta-learning for few-shot image classification. *Advances in neural information processing systems*, 32, 2019. **10**
- [28] Aditya Khosla, Nityananda Jayadevaprakash, Bangpeng Yao, and Li Fei-Fei. Novel dataset for fine-grained image categorization. In *First Workshop on Fine-Grained Visual Categorization, IEEE Conference on Computer Vision and Pattern Recognition*, Colorado Springs, CO, June 2011. **9, 12**
- [29] Jongmin Kim, Taesup Kim, Sungwoong Kim, and Chang D. Yoo. Edge-labeling graph neural network for few-shot learning. In *The IEEE Conference on Computer Vision and Pattern Recognition (CVPR)*, June 2019. **2**
- [30] Thomas N. Kipf and Max Welling. Semi-supervised classification with graph convolutional networks. In *International Conference on Learning Representations*, 2017. **2**
- [31] Johannes Klicpera, Aleksandar Bojchevski, and Stephan Gunnemann. Predict then propagate: Graph neural networks meet personalized pagerank. In *International Conference on Learning Representations*, 2019. **2**
- [32] Gregory Koch, Richard Zemel, and Ruslan Salakhutdinov. Siamese neural networks for one-shot image recognition. In *ICML Deep Learning Workshop*, volume 2, 2015. **2, 9**
- [33] Martin Koestinger, Martin Hirzer, Paul Wohlhart, Peter M Roth, and Horst Bischof. Large scale metric learning from equivalence constraints. In *2012 IEEE conference on computer vision and pattern recognition*, pages 2288–2295. IEEE, 2012. **1, 2**
- [34] Piotr Koniusz, Anoop Cherian, and Fatih Porikli. Tensor representations via kernel linearization for action recognition from 3d skeletons. In *European conference on computer vision*, pages 37–53. Springer, 2016. **1, 3**
- [35] Piotr Koniusz, Yusuf Tas, and Fatih Porikli. Domain adaptation by mixture of alignments of second-or higher-order scatter tensors. In *Proceedings of the IEEE Conference on Computer Vision and Pattern Recognition*, pages 4478–4487, 2017. **1, 3**
- [36] Piotr Koniusz, Yusuf Tas, Hongguang Zhang, Mehrtash Harandi, Fatih Porikli, and Rui Zhang. Museum exhibit identification challenge for the supervised domain adaptation and beyond. In *Proceedings of the European conference on computer vision (ECCV)*, pages 788–804, 2018. **9**
- [37] Piotr Koniusz, Lei Wang, and Anoop Cherian. Tensor representations for action recognition. *TPAMI*, 2020. **1, 3**
- [38] P. Koniusz, F. Yan, P. Gosselin, and K. Mikolajczyk. Higher-order Occurrence Pooling on Mid- and Low-level Features: Visual Concept Detection. *Technical Report*, 2013. **1, 3**
- [39] Piotr Koniusz, Fei Yan, Philippe-Henri Gosselin, and Krystian Mikolajczyk. Higher-order occurrence pooling for bags-of-words: Visual concept detection. *IEEE transactions on pattern analysis and machine intelligence*, 39(2):313–326, 2016. **1, 3**
- [40] Piotr Koniusz, Fei Yan, and Krystian Mikolajczyk. Comparison of mid-level feature coding approaches and pooling strategies in visual concept detection. *Computer vision and image understanding*, 117(5):479–492, 2013. **3**
- [41] Piotr Koniusz and Hongguang Zhang. Power normalizations in fine-grained image, few-shot image and graph classification. *TPAMI*, 2020. **1, 3**
- [42] Piotr Koniusz, Hongguang Zhang, and Fatih Porikli. A deeper look at power normalizations. In *Proceedings of the IEEE Conference on Computer Vision and Pattern Recognition*, pages 5774–5783, 2018. **1, 2, 3**
- [43] Jonathan Krause, Michael Stark, Jia Deng, and Li Fei-Fei. 3d object representations for fine-grained categorization. In *4th International IEEE Workshop on 3D Representation and Recognition (3dRR-13)*, Sydney, Australia, 2013. **9, 12**
- [44] H. Kuehne, H. Jhuang, E. Garrote, T. Poggio, and T. Serre. HMDB: a large video database for human motion recognition. In *Proceedings of the International Conference on Computer Vision (ICCV)*, 2011. **9, 12**
- [45] Brenden Lake, Ruslan Salakhutdinov, Jason Gross, and Joshua Tenenbaum. One shot learning of simple visual concepts. *Proceedings of the annual meeting of the cognitive science society*, 33(33), 2011. **2, 9**
- [46] Kwonjoon Lee, Subhansu Maji, Avinash Ravichandran, and Stefano Soatto. Meta-learning with differentiable convex optimization. In *Proceedings of the IEEE Conference on Computer Vision and Pattern Recognition*, pages 10657–10665, 2019. **10**
- [47] Zhenguo Li, Fengwei Zhou, Fei Chen, and Hang Li. Meta-sgd: Learning to learn quickly for few shot learning. *arXiv preprint arXiv:1707.09835*, 2017. **2**
- [48] Tsung-Yu Lin, Subhansu Maji, and Piotr Koniusz. Second-order democratic aggregation. In *European Conference on Computer Vision*, 2018. **1**
- [49] Tsung-Yu Lin, Aruni RoyChowdhury, and Subhansu Maji. Bilinear cnn models for fine-grained visual recognition. In *Proceedings of the IEEE international conference on computer vision*, pages 1449–1457, 2015. **1**
- [50] Yanbin Liu, Juho Lee, Minseop Park, Saehoon Kim, Eunho Yang, Sung Ju Hwang, and Yi Yang. Learning to propagate labels: Transductive propagation network for few-shot learning. In *International Conference on Learning Representations*, 2018. **10**
- [51] Ashish Mishra, Vinay Kumar Verma, M Shiva Krishna Reddy, S Arulkumar, Piyush Rai, and Anurag Mittal. A generative approach to zero-shot and few-shot action recognition. In *2018 IEEE Winter Conference on Applications of Computer Vision (WACV)*, pages 372–380. IEEE, 2018. **3**
- [52] Mathew Monfort, Alex Andonian, Bolei Zhou, Kandan Ramakrishnan, Sarah Adel Bargal, Tom Yan, Lisa Brown, Quanfu Fan, Dan Gutfrueud, Carl Vondrick, and Aude Oliva. Moments in time dataset: one million videos for event understanding, 2019. **9, 12**
- [53] Alex Nichol, Joshua Achiam, and John Schulman. On first-order meta-learning algorithms. *arXiv preprint*

- arXiv:1803.02999*, 2018. **2, 10, 11**
- [54] M-E. Nilsback and A. Zisserman. Automated flower classification over a large number of classes. In *Proceedings of the Indian Conference on Computer Vision, Graphics and Image Processing*, Dec 2008. **9**
- [55] Boris Oreshkin, Pau Rodríguez López, and Alexandre Lacoste. Tadam: Task dependent adaptive metric for improved few-shot learning. In *Advances in Neural Information Processing Systems*, pages 721–731, 2018. **10**
- [56] Z. Peng, Z. Li, J. Zhang, Y. Li, G. Qi, and J. Tang. Few-shot image recognition with knowledge transfer. In *2019 IEEE/CVF International Conference on Computer Vision (ICCV)*, pages 441–449, 2019. **2, 10**
- [57] Aniwat Phaphuangwittayakul, Yi Guo, and Fangli Ying. Fast adaptive meta-learning for few-shot image generation. *IEEE Transactions on Multimedia*, 2021. **2**
- [58] F. Porikli and O. Tuzel. Covariance tracker. *CVPR*, 2006. **1, 3**
- [59] S. Rahman, L. Wang, C. Sun, and L. Zhou. Redro: Efficiently learning large-sized spd visual representation. In *European Conference on Computer Vision*, 2020. **1**
- [60] Jagath Chandana Rajapakse and Lipo Wang. *Neural Information Processing: Research and Development*. Springer-Verlag Berlin and Heidelberg GmbH & Co. KG, 2004. **2**
- [61] Mengye Ren, Renjie Liao, Ethan Fetaya, and Richard S Zemel. Incremental few-shot learning with attention attractor networks. *arXiv preprint arXiv:1810.07218*, 2018. **10**
- [62] Mengye Ren, Eleni Triantafillou, Sachin Ravi, Jake Snell, Kevin Swersky, Joshua B. Tenenbaum, Hugo Larochelle, and Richard S. Zemel. Meta-learning for semi-supervised few-shot classification. In *Proceedings of 6th International Conference on Learning Representations ICLR*, 2018. **9, 10**
- [63] Andrés Romero, Michèle Gouiffès, and Lionel Lacassagne. Enhanced local binary covariance matrices (elbmc) for texture analysis and object tracking. In *Proceedings of the 6th international conference on computer vision/computer graphics collaboration techniques and applications*, pages 1–8, 2013. **3**
- [64] Olga Russakovsky, Jia Deng, Hao Su, Jonathan Krause, Sanjeev Satheesh, Sean Ma, Zhiheng Huang, Andrej Karpathy, Aditya Khosla, Michael Bernstein, et al. Imagenet large scale visual recognition challenge. *International journal of computer vision*, 115(3):211–252, 2015. **2**
- [65] Andrei A. Rusu, Dushyant Rao, Jakub Sygnowski, Oriol Vinyals, Razvan Pascanu, Simon Osindero, and Raia Hadsell. Meta-learning with latent embedding optimization. In *International Conference on Learning Representations*, 2019. **2**
- [66] Adam Santoro, David Raposo, David GT Barrett, Mateusz Malinowski, Razvan Pascanu, Peter Battaglia, and Timothy Lillicrap. A simple neural network module for relational reasoning. In *Proceedings of the 31st International Conference on Neural Information Processing Systems*, pages 4974–4983, 2017. **1**
- [67] Victor Garcia Satorras and Joan Bruna Estrach. Few-shot learning with graph neural networks. In *International Conference on Learning Representations*, 2018. **2, 10**
- [68] Ya-Fang Shih, Yang-Ming Yeh, Yen-Yu Lin, Ming-Fang Weng, Yi-Chang Lu, and Yung-Yu Chuang. Deep co-occurrence feature learning for visual object recognition. In *Proceedings of the IEEE Conference on Computer Vision and Pattern Recognition*, pages 4123–4132, 2017. **1, 3**
- [69] Xiangbo Shu, Guo-Jun Qi, Jinhui Tang, and Jingdong Wang. Weakly-shared deep transfer networks for heterogeneous-domain knowledge propagation. In *Proceedings of the 23rd ACM international conference on Multimedia*, pages 35–44, 2015. **2**
- [70] Xiangbo Shu, Jinhui Tang, Guojun Qi, Wei Liu, and Jian Yang. Hierarchical long short-term concurrent memory for human interaction recognition. *IEEE transactions on pattern analysis and machine intelligence*, 2019. **3**
- [71] Xiangbo Shu, Liyan Zhang, Yunlian Sun, and Jinhui Tang. Host–parasite: Graph lstm-in-lstm for group activity recognition. *IEEE transactions on neural networks and learning systems*, 32(2):663–674, 2020. **3**
- [72] Christian Simon, Piotr Koniusz, Richard Nock, and Mehrtash Harandi. On modulating the gradient for meta-learning. In *European Conference on Computer Vision*, 2020. **2**
- [73] Jake Snell, Kevin Swersky, and Richard Zemel. Prototypical networks for few-shot learning. In *Proceedings of the 31st International Conference on Neural Information Processing Systems*, pages 4080–4090, 2017. **1, 2, 9, 10, 11**
- [74] Ge Song and Xiaoyang Tan. Real-world cross-modal retrieval via sequential learning. *IEEE Transactions on Multimedia*, 23:1708–1721, 2021. **2**
- [75] Khurram Soomro, Amir Roshan Zamir, and Mubarak Shah. Ucf101: A dataset of 101 human actions classes from videos in the wild. *arXiv preprint arXiv:1212.0402*, 2012. **9, 12**
- [76] Jong-Chyi Su, Subhransu Maji, and Bharath Hariharan. When does self-supervision improve few-shot learning? In *European Conference on Computer Vision*, pages 645–666. Springer, 2020. **2, 10**
- [77] Ke Sun, Piotr Koniusz, and Zhen Wang. Fisher-bures adversary graph convolutional networks. *UAI*, 115:465–475, 2019. **2**
- [78] Flood Sung, Yongxin Yang, Li Zhang, Tao Xiang, Philip HS Torr, and Timothy M Hospedales. Learning to compare: Relation network for few-shot learning. In *Proceedings of the IEEE conference on computer vision and pattern recognition*, pages 1199–1208, 2018. **1, 2, 4, 9, 10, 11, 12**
- [79] Christian Szegedy, Wei Liu, Yangqing Jia, Pierre Sermanet, Scott Reed, Dragomir Anguelov, Dumitru Erhan, Vincent Vanhoucke, and Andrew Rabinovich. Going deeper with convolutions. In *The IEEE Conference on Computer Vision and Pattern Recognition (CVPR)*, 2015. **1**
- [80] Jinhui Tang, Xiangbo Shu, Zechao Li, Guo-Jun Qi, and Jingdong Wang. Generalized deep transfer networks for knowledge propagation in heterogeneous domains, 2016. **2**
- [81] Jinhui Tang, Xiangbo Shu, Rui Yan, and Liyan Zhang. Coherence constrained graph lstm for group activity recognition. *IEEE transactions on pattern analysis and machine intelligence*, 2019. **3**
- [82] Lei Tang and Huan Liu. Relational learning via latent social dimensions. In *Proceedings of the 15th ACM SIGKDD international conference on Knowledge discovery and data mining*, pages 817–826, 2009. **2**
- [83] Oncel Tuzel, Fatih Porikli, and Peter Meer. Region covariance: A fast descriptor for detection and classification. In *European conference on computer vision*, pages 589–600. Springer, 2006. **1, 3**
- [84] Oriol Vinyals, Charles Blundell, Timothy Lillicrap, Koray Kavukcuoglu, and Daan Wierstra. Matching networks for one shot learning. In *Proceedings of the 30th International Conference on Neural Information Processing Systems*, pages 3637–3645, 2016. **1, 2, 9, 11**
- [85] C. Wah, S. Branson, P. Welinder, P. Perona, and S. Belongie. The Caltech-UCSD Birds-200-2011 Dataset. Technical Report CNS-TR-2011-001, California Institute of Technology, 2011. **9, 12**
- [86] Lei Wang, Jun Liu, and Piotr Koniusz. 3d skeleton-based few-shot action recognition with jeanie is not so naïve, 2021. **2, 3**
- [87] Qing Wang, Feng Chen, and Wenli Xu. Tracking by third-order tensor representation. *Systems, Man, and Cybernetics, Part B: Cybernetics, IEEE Transactions on*, 41(2):385–396, 2011. **1**
- [88] Xianjing Wang, Flora D. Salim, Yongli Ren, and Piotr Koniusz. Relation embedding for personalised translation-based poi recommendation. *Lecture Notes in Computer Science*, page 53–64, 2020. **2**
- [89] Yan Wang, Wei-Lun Chao, Kilian Q Weinberger, and Laurens van der Maaten. Simpleshot: Revisiting nearest-neighbor classification for few-shot learning. *arXiv preprint arXiv:1911.04623*, 2019. **10**
- [90] Kilian Q Weinberger, John Blitzer, and Lawrence K Saul.

- Distance metric learning for large margin nearest neighbor classification. In *Advances in neural information processing systems*, pages 1473–1480, 2006. [1](#), [2](#)
- [91] R. S. Woodworth and E. L. Thorndike. The influence of improvement in one mental function upon the efficiency of other functions. *Psychological Review* (1), 8(3):247–261, 1901. [2](#)
- [92] Felix Wu, Tianyi Zhang, Amauri Holanda de Souza Jr., Christopher Fifty, Tao Yu, and Kilian Q. Weinberger. Simplifying graph convolutional networks. In *ICML*, 2019. [2](#)
- [93] Baohan Xu, Hao Ye, Yingbin Zheng, Heng Wang, Tianyu Luwang, and Yu-Gang Jiang. Dense dilated network for few shot action recognition. In *Proceedings of the 2018 ACM on International Conference on Multimedia Retrieval*, pages 379–387. ACM, 2018. [3](#)
- [94] Haohang Xu, Hongkai Xiong, and Guojun Qi. Flat: Few-shot learning via autoencoding transformation regularizers. *arXiv preprint arXiv:1912.12674*, 2019. [2](#), [10](#)
- [95] Jia yu Zhang, Chenglong Zhao, Bingbing Ni, Minghao Xu, and X. Yang. Variational few-shot learning. *2019 IEEE/CVF International Conference on Computer Vision (ICCV)*, pages 1685–1694, 2019. [10](#)
- [96] Chi Zhang, Yujun Cai, Guosheng Lin, and Chunhua Shen. Deepemd: Few-shot image classification with differentiable earth mover’s distance and structured classifiers. In *Proceedings of the IEEE/CVF Conference on Computer Vision and Pattern Recognition*, pages 12203–12213, 2020. [7](#), [10](#)
- [97] Hongguang Zhang and Piotr Koniusz. Power normalizing second-order similarity network for few-shot learning. In *2019 IEEE Winter Conference on Applications of Computer Vision (WACV)*, pages 1185–1193, 2019. [2](#), [11](#)
- [98] Hongguang Zhang, Piotr Koniusz, Songlei Jian, Hongdong Li, and Philip H. S. Torr. Rethinking class relations: Absolute-relative supervised and unsupervised few-shot learning. In *Proceedings of the IEEE/CVF Conference on Computer Vision and Pattern Recognition (CVPR)*, pages 9432–9441, June 2021. [2](#), [10](#)
- [99] Hongguang Zhang, Jing Zhang, and Piotr Koniusz. Few-shot learning via saliency-guided hallucination of samples. In *Proceedings of the IEEE Conference on Computer Vision and Pattern Recognition*, pages 2770–2779, 2019. [2](#), [10](#)
- [100] Hongguang Zhang, Li Zhang, Xiaojuan Qi, Hongdong Li, Philip HS Torr, and Piotr Koniusz. Few-shot action recognition with permutation-invariant attention. In *Computer Vision—ECCV 2020: 16th European Conference, Glasgow, UK, August 23–28, 2020, Proceedings, Part V 16*, pages 525–542. Springer, 2020. [3](#), [9](#), [11](#), [12](#)
- [101] Jianjia Zhang, Lei Wang, Luping Zhou, and Wanqing Li. Beyond covariance: SICE and kernel based visual feature representation. *Int. J. Comput. Vis.*, 129(2):300–320, 2021. [1](#)
- [102] Bolei Zhou, Aditya Khosla, Agata Lapedriza, Aude Oliva, and Antonio Torralba. Learning deep features for discriminative localization. In *Proceedings of the IEEE conference on computer vision and pattern recognition*, pages 2921–2929, 2016. [7](#)
- [103] Hao Zhu and Piotr Koniusz. Simple spectral graph convolution. In *International Conference on Learning Representations (ICLR)*, 2021. [2](#)
- [104] Kai Zhu, Yang Cao, Wei Zhai, and Zheng-Jun Zha. One-shot texture retrieval using global grouping metric. *IEEE Transactions on Multimedia*, 2020. [2](#)
- [105] Linchao Zhu and Yi Yang. Compound memory networks for few-shot video classification. In *The European Conference on Computer Vision (ECCV)*, September 2018. [3](#), [11](#), [12](#)
- [106] Yaohui Zhu, Chenlong Liu, and Shuqiang Jiang. Multi-attention meta learning for few-shot fine-grained image recognition. In *IJCAI*, pages 1090–1096, 2020. [11](#), [12](#)
- [107] Yaohui Zhu, Weiqing Min, and Shuqiang Jiang. Attribute-guided feature learning for few-shot image recognition. *IEEE Transactions on Multimedia*, 2020. [2](#)

- [108] Luisa Zintgraf, Kyriacos Shiarli, Vitaly Kurin, Katja Hofmann, and Shimon Whiteson. Fast context adaptation via meta-learning. In *International Conference on Machine Learning*, pages 7693–7702, 2019. [2](#)



interests include fine-grained image classification, zero-shot learning, few-shot learning and deep learning methods.

**Hongguang Zhang** Hongguang Zhang is currently an assistant professor in Systems Engineering Institute, AMS. Before this, he received his PhD degree in computer vision and machine learning at the Australian National University and Data61/CSIRO, Canberra, Australia in 2020. He received the BSc degree in electrical engineering and automation from Shanghai Jiao Tong University, Shanghai, China in 2014. He received his MSc degree in electronic science and technology from National University of Defense Technology, Changsha, China in 2016. His



Prize Honorable Mention in 2017.

**Hongdong Li** was with NICTA Canberra Labs, prior to 2010, where he involved in the “Australia Bionic Eyes” Project. He is currently a Professor with the Computer Vision Group, The Australian National University. He is also a Chief Investigator of the Australia ARC Centre of Excellence for Robotic Vision. His research interests include 3D vision reconstruction, structure from motion, multi-view geometry, as well as applications of optimization methods in computer vision. He was a recipient of the CVPR Best Paper Award in 2012 and the Marr



ization, spectral learning on graphs and tensors, kernel methods and deep learning.

**Piotr Koniusz** A Senior Research Scientist in Machine Learning Research Group at Data61/CSIRO, formerly known as NICTA, and a Senior Honorary Lecturer at Australian National University (ANU). Previously, he worked as a postdoctoral researcher in the team LEAR, INRIA, France. He received his BSc degree in Telecommunications and Software Engineering in 2004 from the Warsaw University of Technology, Poland, and completed his PhD degree in Computer Vision in 2013 at CVSSP, University of Surrey, UK. His interests include visual categorization, spectral learning on graphs and tensors, kernel methods and deep learning.